

# **Terrain Influences on Synoptic Storm Structure and Mesoscale Precipitation Distribution during IPEX IOP3**

Jason C. Shafer

NOAA Cooperative Institute for Regional Prediction and Department of Meteorology, University  
of Utah, Salt Lake City, Utah

W. James Steenburgh

NOAA Cooperative Institute for Regional Prediction and Department of Meteorology, University  
of Utah, Salt Lake City, Utah

Justin A. W. Cox

NOAA Cooperative Institute for Regional Prediction and Department of Meteorology, University  
of Utah, Salt Lake City, Utah

John P. Monteverdi

San Francisco State University, San Francisco, California

Submitted to *Monthly Weather Review*

November 22, 2004

---

Corresponding author address:

Jason C. Shafer

University of Utah

Department of Meteorology

135 South 1460 East Room 819

Salt Lake City, UT 84112-0110

jshafer@met.utah.edu

## **Abstract**

The influence of topography on the evolution of a winter storm over the western United States and distribution of precipitation over northern Utah are examined using data collected during IOP3 of the Intermountain Precipitation Experiment (IPEX). The analysis is based on high-density surface observations collected by the MesoWest cooperative networks, special radiosonde observations, wind profiler observations, NEXRAD radar data, and conventional data. A complex storm evolution was observed, beginning with frontal distortion and low-level frontolysis as a surface occluded front approached the Sierra Nevada. As the low-level occluded front weakened, the associated upper-level trough moved over the Sierra Nevada and overtook a lee trough. The upper-level trough, which was forward sloping and featured more dramatic moisture than temperature gradients, then moved across Nevada with a weak surface reflection as a pressure trough.

Over northern Utah, detailed observations revealed the existence of a midlevel trough beneath the forward-sloping upper-level trough. This midlevel trough appeared to form along a high potential vorticity banner that developed over the southern Sierra Nevada and was advected downstream over northern Utah. A surface pressure trough moved over northern Utah 3 h after the midlevel trough and delineated two storm periods. Ahead of the surface trough, orographic precipitation processes dominated and produced enhanced mountain precipitation. This period also featured lowland precipitation enhancement upstream of the northern Wasatch Mountains where a windward convergence zone was present. To the south, however, precipitation shadowing produced by the Oquirrh and Stansbury Mountains lowered precipitation amounts across the Salt Lake and Tooele Valleys. Precipitation behind the surface trough was initially dominated by orographic processes, but soon thereafter featured convective precipitation that was not fixed to the terrain. Processes responsible for the complex vertical trough structure and precipitation distribution over northern Utah are discussed.

## 1. Introduction

A major winter storm affected much of the western United States on 12–13 February 2000. Across the lowlands of north-central California, heavy rains produced flooding, the collapse of a Home Depot roof in Colma, and more than 2 million dollars of damage (NCDC 2000, p. 29). Mountain snows of 60–120 cm (2–4 ft) fell over the Sierra Nevada, and prefrontal wind gusts reaching  $26 \text{ m s}^{-1}$  uprooted trees across parts of southern California (NCDC 2000, p. 26–27). Over northern Utah, the storm was responsible for 60–90 cm of mountain snow, and up to 2.1 cm of snow water equivalent (SWE) at lowland locations. Significant precipitation gradients were observed over northern Utah. For example, the mountain site Snowbasin (SNI, 2256 m) recorded 4.9 cm SWE, over twice the 2.1 cm which fell at Ogden (OGD, 1360m), a lowland site only 15 km away. In addition, significant precipitation contrasts were observed between sites at comparable elevations. For example, the 2.1 cm of SWE at OGD was nearly four times greater than the 0.6 cm observed 45 km away at Salt Lake City (SLC, 1280 m). The storm system also featured a complex evolution from landfall along the California coast to the interior Intermountain region, including the development of a complex vertical trough structure over the Sierra Nevada and Great Basin (Shafer 2002; Schultz et al. 2002).

This event occurred during the third intensive observing period (IOP3) of the Intermountain Precipitation Experiment (IPEX, Schultz et al. 2002), a research program designed to improve the understanding and prediction of precipitation over the Intermountain region of the western United States. IOP3 was characteristic of many Intermountain cool-season storms where a landfalling Pacific storm system weakened and underwent a complex evolution across the Intermountain region. As will be discussed further within this paper, the storm's evolution and precipitation producing mechanisms were intrinsically related to the complex topography of the Intermountain region, which is characterized by basin-and-range terrain where narrow, steeply sloped mountain ranges are separated by broad lowland valleys and basins (Fig. 1a). For example, northern Utah features the meridionally oriented Stansbury, Oquirrh, and Wasatch Mountains, which rise 1500–2000 m above the surrounding lowlands (Fig. 1b).

This paper intends to advance the understanding of cool-season Intermountain storm systems through two objectives. The first is to describe the large-scale storm evolution from the Pacific coast to northern Utah, with emphasis on the surface and vertical structure. The second objective is to examine the precipitation distribution over northern Utah and its relationship to the interaction of the kinematic and thermodynamic structure of the storm with local topography. The vertical structure of this system underwent dramatic change from California to Utah, and the precipitation distribution across northern Utah featured both similarities and departures from climatological precipitation versus altitude relationships. Readers are referred to Cox et al. (2004) for a detailed analysis of the kinematic structure of this event near the Wasatch Mountains, and Colle et al. (2004) for a microphysical analysis and numerical simulation of this event.

## **2. Data and methods**

The analyses presented in this paper were performed using a variety of field program and conventional datasets. Surface observations were provided by the MesoWest cooperative networks (Horel et al. 2002), including data from approximately 2500 stations in the western United States and 250 stations across northern Utah. MesoWest observations were quality controlled by comparing the observed values to an estimate based on multivariate linear regression (Splitt and Horel 1998), and by spatial and temporal consistency checks performed while preparing manual analyses. Precipitation observations were quality controlled by Cheng (2001), and generally featured 0.01 inch resolution (amounts were converted to cm for publication). For a description of precipitation gauge characteristics see Table 1 in Cox et al. (2004). Special 1-sec Automated Surface Observing System (ASOS) data was also downloaded from National Climatic Data Center (NCDC) and used for the surface time series<sup>1</sup>. Since MesoWest observations are irregularly spaced horizontally and vertically, the Advanced Regional Prediction System Data Assimilation System (ADAS, Lazarus et al. 2002) was used to generate 1-

---

1. Although available at high temporal resolution, the special ASOS temperature observations are only to the nearest degree C.

km gridded analyses of surface convergence and winds over northern Utah.

Gridded data used for most upper-air analyses was provided by the National Centers for Environmental Prediction Rapid Update Cycle (RUC2; Benjamin et al. 1998), which was available at 60-km horizontal and 25-hPa vertical grid spacing. Comparison with observations and other gridded data suggested that these RUC2 analyses provided the best depiction of the overall storm evolution. ETA Data Assimilation System (EDAS) gridded data, however, was used for low-level potential vorticity analyses because it better captured the potential vorticity banners generated downstream of the Sierra Nevada. MesoWest observations, RUC2, and EDAS gridded data were plotted using GEneral Meteorological PAcKage (GEMPAK) software.

Upper-air data included conventional 12-h and special 6- or 3-h radiosonde observations collected by National Weather Service (NWS) upper-air sites. Over northern Utah, 3-h upper-air soundings were also provided by two National Severe Storm Laboratory mobile labs (NSSL4 and NSSL5), which were located 100 km and 10 km upstream of the Wasatch Crest, respectively (Fig. 1b). In addition, 915 MHz wind profiler data was available from Dugway Proving Grounds (DPG, Fig. 1b), about 120 km southwest of SLC, and at sites in California that were operated by the NOAA Environmental Technology Laboratory (e.g., RMD, SAC, Fig. 1a). Flight-level data from the NOAA P-3 research aircraft and Velocity Azimuth Display (VAD) winds from several Next-Generation Radar (NEXRAD) sites were also used, but are not presented.

Western United States Weather Surveillance Radar-1988 Doppler (WSR-88D) radar mosaics were generated from data provided in NEXRAD Information Dissemination Service (NIDS) format (Baer 1991), which has a spatial resolution of 2 km and an approximate reflectivity resolution of 5 dBZ. Many areas of the western United States, such as central Utah, are not well sampled by the NEXRAD network due to beam blockage, poor spatial coverage, and overshooting (e.g., Westrick et al. 1999; Wood et al. 2003). Over northern Utah, WSR-88D radar analyses from Promontory Point (KMTX, see Fig. 1b for location) were based on NIDS-formatted data with a spatial resolution of 1 km and an approximate reflectivity resolution of 5 dBZ.

Manual surface analyses were prepared following the methods described in section 3 of Steenburgh and Blazek (2001), where 1500-m pressure was used rather than sea level pressure since 1500 m is near the mean elevation of Intermountain observing sites. Surface frontal analysis over the Intermountain region is complicated by numerous issues, including but not limited to the effects of thermally and terrain-driven circulations (Stewart et al. 2002), diabatic processes (Schultz and Trapp 2003), and limitations of the observing network (Horel et al. 2002). Nonetheless, the traditional definition of a frontal zone as an elongated area of strong horizontal temperature gradient (e.g., Bluestein 1986; Keyser 1986), with the front as the boundary on the warm side of the zone, was implemented with consideration of the aforementioned difficulties. In addition, as suggested by Sanders (1999), surface potential temperature analyses were used to help determine the existence of fronts and baroclinic troughs in complex terrain, but are not presented in this paper.

### **3. Synoptic evolution and vertical structure**

At 0000 UTC 12 February 2000, an occluded midlatitude cyclone was located off the west coast of the United States with widespread precipitation across central and northern California (Fig. 2d), and extensive cloudiness extending across much of the western United States (Fig. 2c). The associated 500-hPa shortwave trough axis and absolute vorticity maximum were positioned upstream of the surface cyclone (Fig. 2a). The surface occluded front extended equatorward from the low center (Fig. 2d), and, like many California occlusions (e.g., Elliot 1958), behaved more like a cold front. For example, as the occluded front moved across north-central California, 2–4°C surface temperature falls were observed at San Francisco (SFO, Fig. 3a) and Sacramento (SAC, Fig. 3b), and radar imagery revealed that a narrow frontal rainband was coincident with the occluded front and embedded within the large-scale precipitation shield (not shown). The baroclinicity of the occluded front weakened rapidly with height with little temperature contrast at 700 hPa (Fig. 2b). Southwesterly cross barrier flow produced a lee trough east of the Sierra Nevada (Fig. 2d).

The vertical structure of the system was complex. Wind profiler observations near SFO at Richmond (RMD) and SAC (see Fig. 1a for locations) indicated backing winds with height within the low-level frontal zone, which sloped rearward with height (Figs. 4a and 4b). Above the low-level frontal zone, however, the 0300 UTC (all times for 12 February 2000 unless noted) RUC2 analysis showed that the upper-level trough axis sloped forward with height from 600 hPa to 250 hPa, with the leading edge of a weak upper-level baroclinic zone downstream over western Nevada (Fig. 5). The upper-level trough was accompanied by a significant relative humidity gradient, with high relative humidities ahead and lower relative humidities behind. The strongest and deepest upward vertical velocities were located downstream of the trough axis and beneath the upper-level baroclinic zone.

By 0600 UTC, the primary 500-hPa vorticity maximum was positioned off the south-central California coast (Fig. 6a), and a well-defined upper-level trough was evident in satellite imagery (Fig. 6c). A large area of moderate to heavy precipitation was found over central California and the Sierra, while lighter precipitation extended northeastward from north-central Nevada towards southern Idaho (Fig. 6d). A secondary 500-hPa vorticity maximum (Fig. 6a), associated with an upper-level jet streak (not shown), extended downstream across northeast Nevada. As this vorticity maximum approached northern Utah, mid- and upper-tropospheric relative humidities increased (e.g., 700 hPa, Fig. 6b). At 700 hPa, there was little or no temperature advection over central California (Fig. 6b), however, wind profiler observations suggested (Figs. 4a and 4b) that winds were backing with height below 700 hPa, indicating cold advection below 700 hPa. The 1500-m low center had become more diffuse and was located over southwest Oregon (Fig. 6d). The occluded front, which was now detached from the low center, was approaching the windward slopes of the Sierra Nevada (Fig. 6d). Due to the higher mean elevation of the Intermountain region, the remainder of this paper will define vertical levels as follows: low-level from the surface to 700 hPa, mid-level 700–500 hPa, and upper-level above 500 hPa.

From 0600-1200 UTC, the surface front approached the Sierra Nevada and its

thermodynamic and kinematic structure became less coherent as it split around the Sierra Nevada as observed during other events (e.g., Fig. 4.16, Blazek 2000). Specifically, the eastward movement of the surface front was retarded by the central Sierra. The southern portion of the occluded front was deflected equatorward while the northern portion continued eastward (refer to summary Fig. 12a). The front weakened dramatically by the time it moved into the lee of the Sierra. At Reno (RNO, see Fig. 1a for location), a station pressure minimum occurred around 0800 UTC with a 2°C temperature decrease between 0900–1000 UTC, which was coincident with a trace of light rain from 0936–0946 UTC and veering winds from southeasterly to southerly (Fig. 3c). Winds then decreased and shifted to westerly as station pressures began to steadily rise around 1200 UTC. Thus, there was a well-defined wind shift accompanied with a pressure rise at RNO that featured little or no temperature change. The temperature drop preceded the wind shift and was coincident with light rain and presumably evaporative cooling. This evolution may be related to RNO being immediately downstream of the Sierra Nevada; perhaps the deepest cold air was blocked by the Sierra or never arrived due to downslope warming, while a precipitation band associated with mid-level vertical motion was able to traverse the Sierra ahead of the large-scale pressure trough.

By 1200 UTC, the upper-level trough was located downstream of the Sierra Nevada crest over western Nevada, and the upper-level baroclinic zone had weakened (Fig. 7). The upper-level baroclinic zone, mid-level cold advection, and deep tropospheric vertical motion were moving across Nevada and approaching northern Utah (cold advection not shown). Precipitation across most of California had ended, and widespread precipitation was falling across much of the Intermountain region, including the IPEX target area (not shown).

A curious aspect of this event was the rapid movement of the surface pressure trough across Nevada. Between 1200–1800 UTC, the surface pressure trough moved rapidly (20–25 m s<sup>-1</sup>) across Nevada, and generally featured veering surface winds and little or no surface baroclinity. For example, when the surface pressure trough passed Elko (EKO, see Fig. 1a for location) around 1400 UTC, winds were calm, surface temperatures remained steady at 2°C, and light snow

was falling (not shown). The rapid movement was better correlated with the speed of the upper-level trough axis rather than by low-level advection. In fact, the surface pressure trough was nearly coincident with the leading edge of the upper-level trough and the deepest upward vertical velocity (Fig. 8). Thus, the pressure minimum associated with the surface trough was most likely a reflection of upper-level mass divergence and associated vertical motion immediately ahead of the upper-level trough, as observed in other events over the western United States (e.g., Hess and Wagner 1948; Schultz and Doswell 2000).

At 1800 UTC, the primary 500-hPa vorticity maximum was positioned over southern Nevada, and the 500-hPa trough axis had elongated and split, becoming negatively tilted (Fig. 9a). Although the strongest 500-hPa vorticity was located over southern Nevada, the primary surface low pressure center was positioned well to the north, near the Idaho–Oregon border, with a secondary pressure minimum over northwest Wyoming (Fig. 9d). The surface pressure trough, along with widespread clouds and precipitation, was present ahead of and roughly parallel to the 500-hPa trough axis (Fig. 9c). At 700 hPa, higher relative humidity and weak cold advection was generally present over the Intermountain region (Fig. 9b).

As the surface trough moved across northern Utah between 2000–2200 UTC, it developed baroclinity, and will hereon be referred to as the baroclinic trough. Ahead of the baroclinic trough, IPEX scientists were perplexed when mesoscale observations revealed a midlevel trough that arrived ~3 h ahead of the baroclinic trough. The midlevel trough was not accompanied by an abrupt change in temperature or moisture, but rather a small (1–3°C over 2 h) decrease in equivalent potential temperature with respect to ice ( $\theta_{ei}$ ). The midlevel trough appeared to develop along a high potential vorticity banner that developed over the southern Sierra Nevada. Schär et al (2003) and Grubišić (2004) describe the development of similar banners over the Alps and Dinaric Alps. As shown in Figure 10, low and high potential vorticity banners extended downstream from the Sierra at 0600 UTC (Fig. 10a). By 1200 UTC, the southwesterly flow had advected the high potential vorticity banner northeastward into northeast Nevada and northwest Utah (Fig. 10b). The weak mid-level trough appeared to develop along this high potential vorticity

banner as it moved downstream into the Great Salt Lake Basin (Fig. 10c).

By 0000 UTC 13 Feb, the 500-hPa trough had weakened considerably with the primary vorticity maximum in northeast Arizona (Fig. 11a). A broad region of low 1500-m pressure extended from the Idaho-Montana border southeastward to Wyoming with weak ridging building over Utah (Fig. 11c). Weak 700-hPa cold advection (not shown), clouds and precipitation were present over much of northern Utah (Figs. 11b and 11c), but the precipitation event was close to ending.

Figure 12a and 12b summarize the surface and vertical structure evolution of this event. An occluded mid-latitude cyclone made landfall around 0000 UTC 12 Feb 2000. As the system moved inland, the low pressure area became increasingly diffuse, separated from the surface occluded front, and moved northeastward while the surface occluded front advanced towards the Sierra Nevada. The surface front sloped rearward with height, but the associated upper-level trough was forward-sloping. As the system approached the Sierra, the surface front weakened and split into northern and southern sections, while the upper-level trough and baroclinic zone continued moving eastward. Essentially, the terrain acted to “strip” the low-level occluded front from the upper-level trough. The upper-level trough then coupled with the Sierra lee trough, and the two features moved rapidly downstream across northern Nevada. The rapid movement of the surface trough suggested close coupling with the mass divergence accompanying the upper-level trough. Over northern Utah, these features were preceded by a mid-level trough that formed along a high potential vorticity banner that developed over the Sierra Nevada.

#### **4. Mesoscale storm structure over northern Utah**

##### *a) Pre-baroclinic surface trough period 0900–2100 UTC*

Southerly to southwesterly low- and mid-level flow developed over the IPEX target area as the upper-level and surface troughs approached northern Utah. Between 0900–1800 UTC, there was little change to the large-scale kinematic environment which featured southerly low-level flow with an 8–12 m s<sup>-1</sup> wind speed maximum located just below mid-mountain (hereafter

defined as 775 hPa or ~2200 m AMSL) at 800 hPa (Fig. 13). Above this level, winds veered to southwesterly, resulting in a significant cross-barrier flow component at crest level (~700 hPa). In the lowlands, winds were mainly southerly within the valleys upstream of the Wasatch Mountains (Figs. 14a,b). This southerly along-barrier flow (hereafter referred to as valley flow) was oriented normal to the 1500-m isobars (cf. Figs. 9d and 13b) and was highly ageostrophic. Southwesterly flow over and upstream of the Great Salt Lake became confluent with the along-barrier flow near the eastern shore of the Great Salt Lake. ADAS analyses showed that this region of confluent flow was convergent (Fig. 15), and it will hereon be referred to as a windward convergence zone.

Precipitation began to fall at mountain locations by ~0900 UTC as the large-scale upward vertical motion and moisture ahead of the upper-level trough overspread northern Utah (Fig. 16a). Precipitation onset was delayed up to 3h at many lowland sites (e.g., SNX and SLC, Fig. 16b). This delay appeared to be the result of low-level sublimation and evaporation as suggested by the 0600 and 1200 UTC soundings from SLC which showed a descending cloud base with the 775–600 hPa lapse rate approaching the pseudo adiabat (Fig. 17). By 1200 UTC, vertical profiles of potential temperature ( $\theta$ ) and equivalent potential temperature with respect to ice ( $\theta_{ei}$ ) showed that, with the exception of a shallow layer near 800 hPa,  $\theta$  increased with height from the surface to 500 hPa, but  $\theta_{ei}$  was nearly constant with height up to 575 hPa, indicating near-neutral stability for ice-saturated ascent (Fig. 18a). By 1800 UTC, this near-neutral layer extended to ~500 hPa at both near-barrier sounding locations (SLC and NSSL5, Figs. 18a,b).

Precipitation during this period was generally widespread with some weak convective elements; 0.5° base reflectivities were no greater than 35dbz (e.g. Fig. 19a). Animation of radar reflectivity showed some transient precipitation features, but by in large the precipitation was fixed to the terrain. This suggested that precipitation processes were strongly influenced by the regional orography. For example, radar imagery at 1900 UTC 12 Feb showed an area of locally high reflectivity upstream of the Wasatch Mountains near OGD, whereas lower reflectivities (often below 5 dBZ) were found over the Salt Lake Valley (Fig. 19b). Although beam blockage and other radar limitations prevented analysis of the KMTX reflectivity structure directly over the

Wasatch Mountains, a narrow reflectivity maximum was observed directly over the barrier crest by the NOAA WP-3D tail radar (see Cox et al. 2004).

Precipitation gauge observations from five northern Utah locations, including two mountain sites (CLN and SNI) and three lowland sites (OGD, SNX, and SLC, see Fig. 1b for locations), further illustrate the orographic influences on the precipitation distribution. Although blocking of the large-scale southwesterly flow by the Wasatch and other ranges resulted in southerly along-barrier flow at low levels (e.g., Fig. 14, Cox et al. 2004), sufficient ( $5\text{--}10\text{ m s}^{-1}$ ) cross barrier flow at mid-mountain and crest level (Fig. 20, 1800 UTC traces) produced a substantial orographic enhancement. By 2100 UTC, SNI and CLN reported 2.4 cm and 3.0 cm SWE, respectively (Fig. 16c), with fairly constant precipitation rates reaching  $4\text{ mm h}^{-1}$  (Fig. 16b). Precipitation at SNI (CLN) was roughly double (thirty) times that at nearby low elevation OGD (SLC).

In the lowlands immediately upstream of the Wasatch Mountains, significant precipitation contrasts were observed between OGD, SNX, and SLC. Only 0.1 cm of rain fell at SLC (surface temperatures were  $4\text{--}5^{\circ}\text{C}$ ) through 2100 UTC, whereas Ogden (OGD) and Antelope Island (SNX), which are located 30–40 km north of SLC and upstream of the northern Wasatch mountains, recorded much more with 1.6 cm and 1.1 cm, respectively (Fig. 16a). At least two factors contributed to this lowland precipitation contrast. One, the subcloud evaporation and rain shadowing over the Salt Lake Valley, as discussed in the next paragraph; two, windward convergence and precipitation enhancement in the vicinity of OGD.

Precipitation at OGD and SNX was coincident with a saturated low-level environment as indicated on the 1800 UTC NSSL5 sounding (Fig. 21). In contrast, the 1800 UTC SLC sounding revealed a much a drier low-level environment that likely reduced precipitation amounts at SLC. The drier low-level environment at SLC, as well as across much of the Salt Lake Valley, appeared to be partially related to downslope flow from the southern terminus of the Salt Lake Valley (e.g., Fig. 14b), which features a traverse mountain range that reaches more than 2000 m, and/or subsidence produced by rainshadowing to the lee of the Oquirrh Mountains. The presence of a

pre-existing dry environment (Fig. 17) also played a role.

Heavier precipitation was observed at OGD and SNX (Figs. 16b,c), which were not strongly influenced by rainshadowing from upstream ranges. These sites were affected also by the windward convergence zone, which enhanced precipitation over the lowlands immediately upstream of the Wasatch Mountains. As illustrated by Figs. 14 and 15, convergence was observed upstream of the Wasatch Mountains where southwesterly flow merged with southerly along-barrier flow. The most significant precipitation enhancement occurred immediately downstream of the convergence zone, as illustrated by the region of high radar reflectivity extending approximately 25 km upstream of the Wasatch Crest near Ogden at 1900 UTC (Fig. 19b). Precipitation rates at OGD reached  $2.5 \text{ mm SWE h}^{-1}$ , which was at times surprisingly similar to the nearby mountain precipitation rate at SNI (cf. Figs. 15a,b). The convergence zone and associated windward precipitation region advanced toward the barrier with the approach of the baroclinic trough, as described in detail by Cox et al. (2004) and Colle et al. (2004).

The storm environment was modified only slightly as the midlevel trough moved across northern Utah between 1800–2100 UTC (Fig. 13). The midlevel trough was marked by veering winds between 700 and 500 hPa. P-3 flight-level data between 700 hPa and 500 hPa revealed there were no abrupt temperature or moisture gradients present across the midlevel trough, but rather a small ( $1\text{--}3^\circ\text{C}$  over 2 h) decrease of mid- and upper-level  $\theta_{ei}$ . No organized precipitation structures were coincident with the midlevel trough, although the confluent flow over the eastern half of the Great Salt Lake advanced toward the Wasatch Mountains during and following its passage (see Cox et al. 2004). During this period, lowland precipitation rates increased slightly or remained steady, but at most mountain stations (1900m ASL and above), precipitation rates remained steady or decreased slightly.

#### *b) Postbaroclinic trough period 2100-0600 UTC*

At 2100 UTC, the surface baroclinic trough was collocated with a weak east-west band of precipitation over the southern end of the Great Salt Lake (Fig. 19c). The baroclinic trough

intensified as it moved across northern Utah, and, at SLC, was accompanied by a 2°C temperature drop, surface pressure minimum, and wind shift around 2130 UTC (Fig. 22). The strongest temperature changes with the baroclinic trough over northern Utah were coincident with moderate or heavy precipitation; thus, diabatic processes appeared to produce much of the baroclinity accompanying the trough as it moved into northern Utah, similar to that described by Schultz and Trapp (2003).

The wind changes accompanying the baroclinic trough were complex across northern Utah. At DPG and the immediately adjacent lowlands, surface winds veered from southerly to westerly with baroclinic trough passage (cf. Fig. 14b, Fig. 23). Across the Salt Lake and Tooele Valleys, however, the surface wind shift was weak, or short-lived (Fig. 23), with a few exceptions (e.g., SLC, Fig. 22). Inspection of MesoWest stations around 800 m above valley level, however, revealed that a consistent wind shift was associated with the baroclinic trough just above valley level. This elevated wind shift was continuous, moved east-southeast (confirmed with KMTX velocity data, not shown), and was also coincident with the largest temperature falls, which were 2–4°C between 800–600 hPa, with the most significant drop being 4°C at 650 hPa over 2h. Thus, the most notable temperature and wind direction changes associated with the baroclinic trough were generally elevated, between 800 and 600 hPa, and not at valley level.

Precipitation behind the baroclinic trough grew more convective as the low-levels became increasingly unstable after baroclinic trough passage. Much of the lowland precipitation was associated with two transient mesoscale precipitation areas, one a weakly organized area associated with the baroclinic trough (Fig. 19c), and the second a convective line that passed SLC and produced a 4°C temperature drop about 3 h later (Fig. 22). In fact, turbulence and wind shear accompanying this feature (not shown) were strong enough to abort the P-3's first landing attempt. The convective line developed in the airmass behind the baroclinic trough, which featured  $\theta_{ei}$  decreasing with height up to 675 hPa (Fig. 24a). As the baroclinic trough moved southeast, lowland precipitation rates spiked at different times: OGD around 2100 UTC, SNX at 2200 UTC and SLC at 0000 UTC 13 February (Fig. 16c). Precipitation rates at mountain sites,

however, peaked after the lowland locations, reaching  $4 \text{ mm hr}^{-1}$  at both SNI and CLN between 0000–0100 UTC 13 February (Fig. 16b); these increased mountain precipitation rates were associated with destabilization and increased cross-barrier flow behind the baroclinic trough (Fig. 24b), but also could be a reflection of snow buildup on gauge walls falling into the bottom of the gauge, as discussed in Cox et al. (2004). Precipitation enhancement that previously accompanied the windward convergence zone over the lowlands upstream of the northern Wasatch (e.g., OGD, SNX) ended shortly after passage of the baroclinic trough.

Across the Salt Lake and Tooele Valleys, much of total storm precipitation fell in the postbaroclinic trough environment (e.g., SLC 83%) under northwesterly flow when low-level moisture and instability were maximized. Precipitation at mountain locations, however, was generally evenly distributed throughout the event with CLN and SNI receiving about 40% of their total SWE in the postbaroclinic trough environment. Precipitation at both mountain and valley locations ended by 0600 UTC 13 February, as a drier environment and subsidence behind the upper-level trough developed.

### *c) Analysis of Orographic Precipitation*

Storm-total SWE ratios featured three main spatial precipitation patterns. One, significant precipitation enhancement was observed in the higher elevations. Second, precipitation suppression was observed both to the lee of the Wasatch and Oquirrh mountains, including the Salt Lake and Tooele Valleys. Third, local precipitation enhancement was observed in the lowlands upstream of the northern Wasatch (Fig. 25a).

Precipitation generally increased with altitude in IOP3 (Fig. 25b), which resembled the nearly linear climatological distribution (Fig. 25c). However, unlike the climatological precipitation distribution, IOP3 featured a somewhat bimodal distribution above and below 2100m or at lowland and mountain locations. This bimodal precipitation distribution suggested that significant variations from climatological precipitation versus altitude were present during IOP3. Some of these departures from climatology could be explained by two observed spatial

precipitation patterns: one, precipitation suppression in the lee of the Oquirrh mountains (e.g., SLC), and two, precipitation enhancement in the lowlands upstream of the northern Wasatch (e.g., SNX, OGD). For example, SNX and SLC, which have a similar elevation (1280m), orientation relative to the Wasatch, and climatological annual precipitation (SNX, 45.6 cm, SLC, 42 cm), featured nearly a factor of three SWE difference, SNX (1.5 cm) and SLC (.6 cm). Mountain sites (e.g., SNI, 2256m, 4.9 cm) over the northern Wasatch also featured greater precipitation for their respective elevation compared to CLN (2945m, 5.1 cm).

Precipitation anomaly maps were constructed to further compare climatological and IOP3 spatial precipitation patterns. Since annually averaged precipitation correlates well with altitude over the IPEX target region (Fig. 25c), a linear regression equation was developed to describe the climatological precipitation altitude relationship and is given by  $P = 0.0523 * A - 30.406$ , where  $P$  is the precipitation in cm and  $A$  is the altitude in meters. Analysis of the residuals or anomalies from this predicted value for climatological precipitation are shown in Fig. 26a. Positive anomalies are relatively wet areas for their respective elevations, and include the northern Wasatch mountains, lowlands immediately upstream of the Wasatch, eastern two thirds of the Great Salt Lake, and the northern and eastern Tooele and Salt Lake Valleys (Fig. 26a). Negative anomalies, or areas that are relatively dry for their respective elevations, are present over the Great Salt Lake desert, southern Oquirrh Mountains, and downstream of the Wasatch crest (Fig. 26a).

In order to illustrate departures from the climatological precipitation-altitude relationship during IOP3, the slope of the climatological linear fit was fixed to the IOP3 mean precipitation, with residuals from this line presented in Figure 26b. IOP3 generally featured similar precipitation anomaly patterns to climatology, including positive (wet) anomalies over and upstream of the northern Wasatch and negative (dry) anomalies east of Wasatch (Fig. 26b). However, there were differences between IOP3 and climatological precipitation anomaly patterns over the Salt Lake and Tooele Valleys, where the precipitation amounts were smaller than one would expect climatologically.

## 5. Discussion

### *a) Storm evolution over the western United States*

Very few studies have examined the evolution of a winter storm from the Pacific Coast to the interior Intermountain West. During IPEX IOP3, a landfalling occluded front weakened and deformed as it approached the Sierra Nevada, similar to that observed previously near the Sierra Nevada by Hoffman (1995), Reynolds and Kuciasuskas (1988), and Blazek (2000), as well as upstream of the Appalachians (Schumacher et al. 1996). Ultimately, there was little evidence that the baroclinity associated with the surface based occlusion was able to penetrate into the lowlands to the lee of the Sierra Nevada as the upper-level trough continued to move downstream. Thus, the high topography appeared to "strip" or remove the storm system of its low-level baroclinic structure as it traversed the Sierra Nevada. Destruction of the low-level baroclinity may have also been aided by adiabatic warming to the lee of the Sierra Nevada, as suggested by Hobbs et al. (1996) for frontal evolution in the lee of the Rocky Mountains.

To the lee of the Sierra, the upper-level trough interacted with the lee trough, which became mobile and moved rapidly downstream as the upper-level trough axis approached. The downstream movement of the surface trough appeared to be a reflection of mass-divergence associated with the upper-level trough, consistent with early work by Hess and Wagner (1948) and Schultz and Doswell (2000).

The scenario described above suggests that the low-level occluded front and associated pressure trough did not move continuously across the Sierra Nevada. Instead, the occluded front was blocked by the Sierra Nevada while the upper-level trough moved downstream and interacted with the lee trough. This evolution contrasts with that of many idealized simulations of fronts traversing topography (see Blumen 1992 and Egger and Hoinka 1992 for reviews), which typically assume smooth slopes and modest relief so that the front is able to surmount the mountain barrier. It is, however, roughly consistent with the discontinuous low-level evolution described by Dickinson and Knight (1999) who found that for high mountains, the low-level front is blocked, while the associated upper-level potential vorticity maximum moves downstream and

eventually couples with the leeward low-level cyclonic vorticity maximum.

Another curious aspect of IOP3 is the forward-sloping structure of the upper-level trough. This structure resembles that of damping baroclinic waves (e.g., Spencer et al. 1996) and is consistent with the fact that the cyclone was occluded and weakening as it began to interact with the terrain of the western United States.

Finally, the analysis presented in section 4 illustrates a likely origin of the mid-level trough that perplexed IPEX scientists during IOP3 (Schultz et al. 2002). Southwesterly flow ahead of the approaching storm system produced high and low potential vorticity banners downstream of the southern and northern Sierra Nevada, respectively. These banners were qualitatively similar to potential vorticity banners that form downstream of the European Alps (e.g., Schär et al. 2003, Grubišić 2004). The mid-level trough formed along the high potential vorticity banner as it was advected downstream into northeast Nevada and then eastward into Utah. Thus, it appears that potential vorticity banners that form over the Sierra Nevada may complicate the kinematic structure of winter storms over Nevada and Utah. In this case, however, the mid-level trough appeared to have little effect on precipitation processes.

#### *b) Precipitation distribution over northern Utah*

In general, there is a strong correlation between climatological precipitation and altitude across the Intermountain West. As such, precipitation-altitude relationships are used frequently by meteorologists and hydrologists to predict event or annual precipitation (e.g., Hevesi et al. 1992). Over the IPEX target region, climatological precipitation increases linearly with height (e.g., Alter 1919; Daly et al. 1994; Fig. 25c) with a linear correlation coefficient of 0.70. Large departures from this relationship have been observed, however, for storm total precipitation (e.g., Horel and Gibson 1994; Cheng 2001; Shafer et al. 2002) and within individual storms (e.g., Steenburgh 2003). In addition, as illustrated by Fig. 26a and Peck and Brown (1962), the northern Wasatch Mountains and their immediate upstream lowlands, the eastern two-thirds of the Great Salt Lake, and the northern and eastern Tooele and Salt Lake Valleys are anomalously wet for

their elevations, whereas the Great Salt Lake Desert and areas east of the Wasatch Mountains are anomalously dry. Therefore, in addition to a pronounced precipitation-altitude relationship, there are important mesoscale patterns evident in the regional precipitation climatology.

Precipitation during IOP3 occurred under moist southwesterly flow with near moist-neutral stability. Precipitation was dominated by local terrain processes, which produced enhanced/suppressed precipitation at various locations across northern Utah. Three major precipitation patterns were observed: (1) precipitation enhancement with increased altitude, (2) precipitation suppression in the lee of the Stansbury and Oquirrh Mountains (i.e., the Tooele and Salt Lake Valleys), and (3) precipitation enhancement produced by a windward convergence zone over the lowlands upstream of the northern Wasatch Mountains.

These patterns featured important similarities and differences compared to climatology. Precipitation enhancement in the northern Wasatch Mountains and upstream lowlands was consistent with this region being climatologically wet for its elevation. In contrast, IOP3 was dry relative to climatology over the Salt Lake and Tooele Valleys. These characteristics are consistent with southwesterly flow events based on synoptic experience.

Analyses of departures from climatological precipitation-altitude relationships should be employed to better understand event, seasonal, and long-term precipitation distributions in regions of complex terrain. The construction of precipitation anomaly maps for varying flow directions and stability may be a useful predictive tool since systematic precipitation anomalies can be more easily identified and may help expose the underlying processes responsible for such anomalies. Such anomaly maps may also be useful for bias-correcting numerical model forecasts and would likely improve upon techniques that rely primarily on the climatological precipitation-altitude relationship.

## **6. Summary and Conclusions**

This paper has examined the evolution of a winter storm (IPEX IOP3) over the western United States and its precipitation distribution over northern Utah. The event featured a land-

falling occluded front that weakened and deformed as it approached the Sierra Nevada. The occluded front was unable to surmount the Sierra Nevada as the accompanying forward-sloping upper-level trough moved downstream. This apparent terrain stripping of the low-level frontal structure, combined with the coupling of the upper-level trough with the Sierra Nevada lee trough, represents a discontinuous low-level storm evolution that is roughly consistent with the idealized modeling work of Dickinson and Knight (1999). Eventually, the lee trough moved rapidly downstream and appeared to be a reflection of the mass-divergence downstream of the upper-level trough axis.

As the upper-level trough approached northern Utah, it interacted with a mid-level trough that was associated with a high potential vorticity banner that formed downstream of the southern Sierra Nevada. This produced the complex kinematic structure that perplexed IPEX scientists during IOP3. The passage of the mid-level trough across northern Utah, however, had a limited effect on precipitation processes.

Precipitation during the event was dominated by mesoscale terrain processes and featured a general pattern of increased precipitation with increased altitude. Two important departures from the general precipitation-altitude relationship were found: one, the northern Wasatch Mountains and accompanying lowlands were anomalously wet (the development of a windward convergence zone contributed to the lowland enhancement as described by Cox et al. 2004); two, the Tooele and Salt Lake Valleys were anomalously dry. Analyses of long-term and event-specific departures from the climatological precipitation-altitude relationship illustrated that the former was consistent with climatological precipitation distributions, whereas the latter was not. Widespread use of analyses that illustrate long-term and event-specific departures from climatological precipitation-altitude relationships may prove useful for bias-correcting numerical model forecasts and identifying important mesoscale precipitation patterns that are difficult to identify due to the dominance of altitudinal gradients.

This study represents a rare investigation of winter storm evolution over the western United States. During IOP3, the upper-level trough was able to move relatively unimpeded across

the Sierra Nevada and Great Basin ranges while the low-level occluded front was fully blocked, which resulted in discontinuous low-level storm evolution. These observations could be broadly applied to similar events that feature a landfalling mature midlatitude cyclone in California and move across the Intermountain region as the accompanying baroclinic wave weakens. Namely, low-level structures of midlatitude cyclones across the Intermountain region are strongly dependent upon interactions with the underlying terrain, while upper-level features move more or less unimpeded by the complex underlying terrain. Also, mesoscale, terrain-induced circulations dominated precipitation distribution across northern Utah and included not only direct orographic ascent where more precipitation fell in higher terrain, but also enhanced/suppressed precipitation in nearby lowland areas.

This study illustrates the importance of the Intermountain West's topography on synoptic storm evolution and precipitation. Additional research is needed to better understand the passage of baroclinic systems across the Sierra Nevada, including how the resulting terrain-modified structure affects the development and evolution of precipitation over the downstream Intermountain West.

*Acknowledgments.* Funding for the analysis of IPEX IOP3 was provided by National Science Foundation Grants ATM-0085318 and ATM-0333525, and a series of grants provided by the National Weather Service C-STAR program to the NOAA Cooperative Institute for Regional Prediction at the University of Utah. Comments from Lance Bosart and David Schultz improved this paper. We would like to thank all the individuals and organizations who participated in the planning and execution of IPEX. Thanks to the National Severe Storms Lab for operating the mobile labs and the National Weather Service for supplementing radiosonde observations. Thanks also to David E. White and Paul Neiman of NOAA's Environmental Technology Laboratory (ETL) for providing the California wind profiler data.

## References

- Alter, J. C., 1919: Normal precipitation in Utah. *Mon. Wea. Rev.*, **47**, 633-636.
- Baer, V. E., 1991: The transition from the present radar dissemination system to the NEXRAD Information Dissemination Service (NIDS). *Bull. Amer. Meteor. Soc.*, **72**, 29-33.
- Benjamin, S. G., J. M. Brown, K. J. Brundage, B. E. Schwartz, T. G. Smirnova, T. L. Smith and L. L. Marone, 1998: RUC-2 –The Rapid Update Cycle Version 2. NWS Technical Procedure Bulletin No. 448. NOAA/NWS, 18 pp. [Available from National Weather Service, Office of Meteorology, 1325 East-West Highway, Silver Spring, MD 20910].
- Blazek, T. R., 2000: Analysis of a Great Basin cyclone and attendant mesoscale features. M.S. thesis, Dept. of Meteorology, University of Utah, 122 pp. [Available from Dept. of Meteorology, University of Utah, 145 South 1460 East, Room 819, Salt Lake City, UT 84112-0110.]
- Bluestein, H. B., 1986: Fronts and jet streaks: A theoretical perspective. *Mesoscale Meteorology and Forecasting*. (P. S. Ray, Ed.), Amer. Meteor. Soc., 173-215.
- Blumen, W., 1992: Propagation of fronts and frontogenesis versus frontolysis over orography. *Meteor. Atmos. Phys.*, **48**, 37-50.
- Cheng, L., 2001: Validation of quantitative precipitation forecasts during the Intermountain Precipitation Experiment. M.S. thesis, Dept. of Meteorology, University of Utah, 137 pp. [Available from Dept. of Meteorology, University of Utah, 145 South 1460 East, Rm. 819, Salt Lake City, UT 84112-0110.]
- Colle, B. A., J. B. Wolfe, W. J. Steenburgh, D. E. Kingsmill, J. A. W. Cox, and J. C. Shafer, 2004: High resolution simulations and microphysical validation of an orographic precipitation event over the Wasatch Mountains during IPEX IOP3. Submitted to *Mon. Wea. Rev.*
- Cox, J. A.W, W. J. Steenburgh, D. E. Kingsmill, J. C. Shafer, B. A. Colle, O. Bousquet, B. F. Smull, and H. Cai, 2004: The kinematic structure of a Wasatch Mountain winter storm during IPEX IOP3. *Mon. Wea. Rev.* In press.
- Daly, C., R. P. Neilson, and D. L. Phillips, 1994: A statistical-to-topographic mode for mapping

- climatological precipitation over mountainous terrain. *J. Appl. Met.*, **33**, 140-158.
- Dickinson, M. J., D. Knight, 1999: Frontal interaction with mesoscale topography. *J. Atmos. Sci.*, **56**, 3544-3559.
- Egger, J., and K. P. Hoinka, 1992: Fronts and orography. *Meteor. Atmos. Phys.*, **48**, 3-36.
- Elliott, R. D., 1958: California storm characteristics and weather modification. *J. Meteor.* **15**, 486-493.
- Grubišić, V., 2004: Bora-driven potential vorticity banners over the Adriatic. *Quart. J. Roy. Met. Soc.*, **130**, 2571-2603.
- Hess, S. L., and H. Wagner, 1948: Atmospheric waves in the northwestern United States. *J. Meteor.*, **5**, 1-19.
- Hevesi, J. A., A. L. Flint, and J. D. Istok, 1992: Precipitation estimation in mountainous terrain using multivariate geostatistics. Part II: Isohyetal Maps. *J. Appl. Meteor.*, **31**, 677-688.
- Hobbs, P.V., J.D. Locatelli, and J. E. Martin, 1996: A new conceptual model for cyclones generated in the lee of the Rocky Mountains. *Bull. Amer. Meteor. Soc.*, **77**, 1169-1178.
- Hoffman, E. G., 1995: Evolution and mesoscale structure of fronts in the western United States: A case study. M.S. thesis, Dept. of Earth and Atmospheric Sciences, State University of New York at Albany, 287 pp.
- Horel, J. D., and C. V. Gibson, 1994: Analysis and simulation of a winter storm over Utah. *Wea. Forecasting*, **9**, 479-494.
- Horel, J. D., M. Splitt, L. Dunn, J. Pechmann, B. White, C. Ciliberti, S. Lazarus, J. Slemmer, D. Zaff, and J. Burks, 2002: Mesowest: Cooperative mesonets in the western United States. *Bull. Amer. Meteor. Soc.*, **83**, 211-225.
- Keyser, D., 1986: Atmospheric fronts: An observational perspectives. *Mesoscale Meteorology and Forecasting*. (P. S. Ray, Ed.), Amer. Meteor. Soc., 216-258.
- Lazarus, S. M., C. M. Ciliberti, J. D. Horel and K. A. Brewster, 2002: Near-real-time applications of a mesoscale analysis system to complex terrain. *Wea. Forecasting*, **17**, 971-1000.

- NCDC, 2000: *Storm Data*. Vol. 42, No. 2, 127 pp.
- Peck, E. L., and M. J. Brown, 1962: An approach to the development of isohyetal maps for mountainous areas. *J. Geophys. Res.*, **67**, 681-694.
- Reynolds, D. W., and A. P. Kuciauskas, 1988: Remote and in situ observations of Sierra Nevada winter mountains clouds: Relationship between mesoscale structure, precipitation and liquid water. *J. Appl. Meteor.*, **27**, 140-156.
- Sanders, F., 1999: A proposed method of surface map analysis. *Mon. Wea. Rev.*, **127**, 945-955.
- Schär, C., M. Sprenger, D. Lüthi, Q. Jiang, R. B. Smith, and R. Benoit, 2003: Structure and dynamics of an Alpine potential-vorticity banner. *Quart. J. Roy. Met. Soc.*, **129**, 825-855.
- Schultz, D. M., and C. A. Doswell III, 2000: Analyzing and forecasting Rocky Mountain lee cyclogenesis often associated with strong winds. *Wea. Forecasting*, **15**, 152-173.
- Schultz, D. M., W. J. Steenburgh, R. J. Trapp, J. Horel, D. E. Kingsmill, L. B. Dunn, W. D. Rust, L. Cheng, A. Bansemer, J. Cox, J. Daugherty, D. P. Jorgensen, and J. Meitín, L. Showell, B. F. Smull, K. Tarp, and M. Trainor, 2002: Understanding Utah winter storms: The Intermountain Precipitation Experiment. *Bull. Amer. Meteor. Soc.*, **83**, 190-210.
- Schultz, D. M, and R. J. Trapp, 2003: Nonclassical cold-frontal structure caused by dry subcloud air in northern Utah during the Intermountain Precipitation Experiment (IPEX). *Mon. Wea. Rev.*, **131**, 2222-2246.
- Schumacher, P. N., D. J. Knight, and L. F. Bosart, 1996: Frontal interaction with the Appalachian Mountains. Part I: A climatology. *Mon. Wea. Rev.*, **124**, 2453-2468.
- Shafer, J. C., 2002: Synoptic and mesoscale structure of a Wasatch Mountain winter storm. M. S. thesis, Dept. of Meteorology, University of Utah, 65 pp. [Available from Dept. of Meteorology, University of Utah, 135 South 1460 East, Rm. 819, Salt Lake City, UT 84112-0110]
- Spencer, P. L., Carr, F. H., and Doswell, C. A. 1996: Diagnosis of an amplifying and decaying baroclinic wave using wind profiler data. *Mon. Wea. Rev.*, **124**, 209-223.
- Spitt, M. E., and J. D. Horel, 1998: Use of multivariate linear regression for meteorological data

- analysis and quality assessment in complex terrain. Preprints, *10th Symposium on Meteorological Observations and Instrumentation*, Phoenix AZ, Amer. Meteor. Soc., 359-362.
- Steenburgh, W. J., and T. R. Blazek, 2001: Topographic distortion of a cold front over the Snake River Plain and central Idaho Mountains. *Wea. Forecasting*, **16**, 301-314.
- Steenburgh, W. J., 2003: One hundred inches in one hundred hours: Evolution of a Wasatch Mountain winter storm cycle. *Wea. Forecasting*, **18**, 1018-1036.
- Stewart, J. Q., C. D. Whiteman, W. J. Steenburgh, and X. Bian, 2002: A climatological study of thermally driven wind systems of the U.S. Intermountain West. *Bull. Amer. Meteor. Soc.*, **83**, 699-708.
- Westrick, K. J., C. F. Mass, and B. A. Colle, 1999: The limitations of the WSR-88D radar network for quantitative precipitation measurement over the coastal western United States. *Bull. Amer. Meteor. Soc.*, **80**, 2289-2298.
- Wood, V. T., R. A. Brown, and S. V. Vasiloff, 2003: Improved detection using negative elevation angles for mountaintop WSR-88Ds. Part II: simulations of the three radars covering Utah. *Wea. Forecasting*, **18**, 393-403.

## Figure Captions

Figure 1. Topography and major geographic features of (a) the western United States and (b) northern Utah. Elevation (m) based on scale at lower left in (a). Boxed area in (a) identifies location of IPEX target area in (b).

Figure 2. Upper-level, satellite, surface, and radar analyses at 0000 UTC 12 Feb 2000. (a) RUC2 analysis of 500-hPa geopotential height (every 60 m) and absolute vorticity ( $\times 10^{-5} \text{ s}^{-1}$ , shaded following scale at bottom). (b) RUC2 analysis of 700-hPa temperature (every  $2^\circ\text{C}$ ), wind [full (half) barbs denote 5 (2.5)  $\text{m s}^{-1}$ ], and relative humidity (%), shaded following scale at bottom). (c) Infrared satellite image. (d) NEXRAD radar mosaic (reflectivity scale at left) and manual 1500-m pressure analysis. Station reports include 1500-m pressure (tenths of hPa with leading 8 truncated), and wind [as in (b)].

Figure 3. Meteograms for (a) San Francisco (SFO), (b) Sacramento (SAC), and (c) Reno (RNO). Full (half) barbs denote 5 (2.5)  $\text{m s}^{-1}$ . Arrows identify frontal passage in (a) and (b). See Fig. 1a for locations.

Figure 4. Wind profiler data for 12 February 2000 from (a) Richmond (RMD) and (b) Sacramento (SAC). Full (half) barb denote 5 (2.5)  $\text{m s}^{-1}$ . Meridional wind component plotted every 3  $\text{m s}^{-1}$  as solid lines. Dashed lines denote wind shear accompanying frontal zone. See Fig. 1a for locations.

Figure 5. RUC2 cross section along line AB of Fig. 2b at 0300 UTC 12 Feb. Potential temperature (thin lines every 3K), vertical velocity ( $\omega$ , thick lines every  $3 \times 10^{-1} \text{ Pa s}^{-1}$  with negative contours dashed), wind [full (half) barbs denote 5 (2.5)  $\text{m s}^{-1}$ ], and relative humidity (light, dark shading denote  $>70$  and  $90\%$ , respectively). Upper-level trough axis denoted by heavy dashed line, leading edge of upper-level baroclinic zone denoted by heavy solid line, and surface front position denoted by arrow. Sierra Nevada indicated by S.

Figure 6. Same as Fig. 2 except for 0600 UTC 12 Feb 2000.

Figure 7. Same as Fig. 5 except for 1200 UTC 12 Feb 2000 and arrow denotes surface pressure trough position.

Figure 8. Same as Fig. 5 except for 1800 UTC 12 Feb 2000 and arrow denotes position of surface pressure trough.

Figure 9. Same as Fig. 2 except for 1800 UTC 12 February 2000.

Figure 10. EDAS 700-hPa potential vorticity (every  $1 \times 10^{-7} \text{ m}^2 \text{ s}^{-1} \text{ K kg}^{-1}$ ) and wind (vector scale at lower right). High (low) potential vorticity banners denoted by thick solid (dashed) line. (a) 0600 UTC 12 Feb 2000. (b) 1200 UTC. (c) 1800 UTC.

Figure 11. Same as (a) Fig. 2a, (b) Fig. 2c, and (c) Fig. 2d, except for 0000 UTC 13 Feb 2000.

Figure 12. Summary of surface and vertical structure evolution of IOP3. (a) Surface features every 3 h (conventional symbols) from 0000–2100 UTC 12 Feb 2000. Labels represent hour UTC. (b) Vertical trough structure (roughly along line AB of Fig. 2b) every 3 h. U denotes upper level trough, S surface trough, and M midlevel trough.

Figure 13. Salt Lake City (SLC) time-height section based on 3-h soundings (thick barbs) with RUC2 winds (thin barbs) overlaid.  $\theta_e$  (solid lines, every 3 K), relative humidity (light and dark shading denote  $>70$  and  $90\%$ , respectively), and wind [full (half) barbs denote 5 and (2.5)  $\text{m s}^{-1}$ ]. Dashed lines denote mid-level and surface-based troughs.

Figure 14. Northern Utah manual streamline analysis at (a) 1200 and (b) 1800 UTC 12 Feb 2000. Station data and streamlines for elevations between 1280–2200m AMSL (roughly at and below mid mountain). Full (half) barbs denote 5 (2.5)  $\text{m s}^{-1}$ .

Figure 15. ARPS Data Assimilation System (ADAS) surface analysis at 1800 UTC 12 Feb 2000, surface divergence (light and dark shading denote less than  $-0.25 \times 10^{-4} \text{ s}^{-1}$  and  $-3.0 \times 10^{-4} \text{ s}^{-1}$ , respectively) and wind [full (half) barbs denote 5 (2.5)  $\text{m s}^{-1}$ ].

Figure 16. Precipitation rates and accumulated precipitation at selected locations. (a) Mountain precipitation rates ( $\text{mm h}^{-1}$ ). (b) Lowland precipitation rates ( $\text{mm h}^{-1}$ ). (c) Accumulated precipitation (mm). See Fig. 1b for locations.

Figure 17. Skew  $T$ - $\log p$  diagram [temperature (solid) and dewpoint (dashed)] at SLC for 0600 UTC (black) and 1200 UTC (gray) 12 Feb 2000.

Figure 18. Vertical profiles of potential (left) and equivalent potential temperature with respect to

ice (right) at (a) SLC and (b) NSSL5. See Fig. 1b for locations.

Figure 19. Base ( $0.5^\circ$ ) radar reflectivity from Promontory Point (KMTX) at (a) 1200 UTC 12 Feb, (b) 1900 UTC 12 Feb, and (c) 2100 UTC 12 Feb 2000. Reflectivity scale (dBZ) on right. Dashed line in (c) denotes position of baroclinic trough.

Figure 20. Cross-barrier flow magnitude ( $\text{m s}^{-1}$ ) at NSSL4 and NSSL5 for 1800 and 2100 UTC 12 Feb 2000. See Fig. 1b for locations.

Figure 21. Skew  $T$ -log  $p$  diagram [temperature (solid) and dewpoint (dashed)] at SLC and NSSL5 for 1800 UTC 12 Feb 2000.

Figure 22. Same as in Fig. 3 except for SLC. Arrows denote the passage of the baroclinic trough (dashed) and convective line (solid). See Fig. 1b for location.

Figure 23. Same as Fig. 14 except for 2200 UTC 12 Feb 2000.

Figure 24. (a) Vertical profiles of potential and equivalent potential temperature with respect to ice at NSSL4 at 2100 and 0300 UTC 13 Feb. (b) NSSL5 cross barrier flow at 2100 and 0300 UTC 13 Feb.

Figure 25. IOP3 precipitation characteristics. (a) Total accumulated liquid precipitation during IOP3 (every 10 mm) with observations annotated; selected contour lines omitted for clarity. (b) Observed liquid precipitation (cm) versus elevation over the IPEX target area. (c) Climatological liquid precipitation (cm) versus altitude over the IPEX target area.

Figure 26. Climatological and observed precipitation anomalies. (a) Climatological precipitation anomaly (cm) relative to linear fit. (b) IOP3 observed precipitation anomaly (mm) relative to the slope of a linear fit to climatological precipitation versus altitude given in Fig. 25c. Selected contour lines omitted for clarity.

## Figures

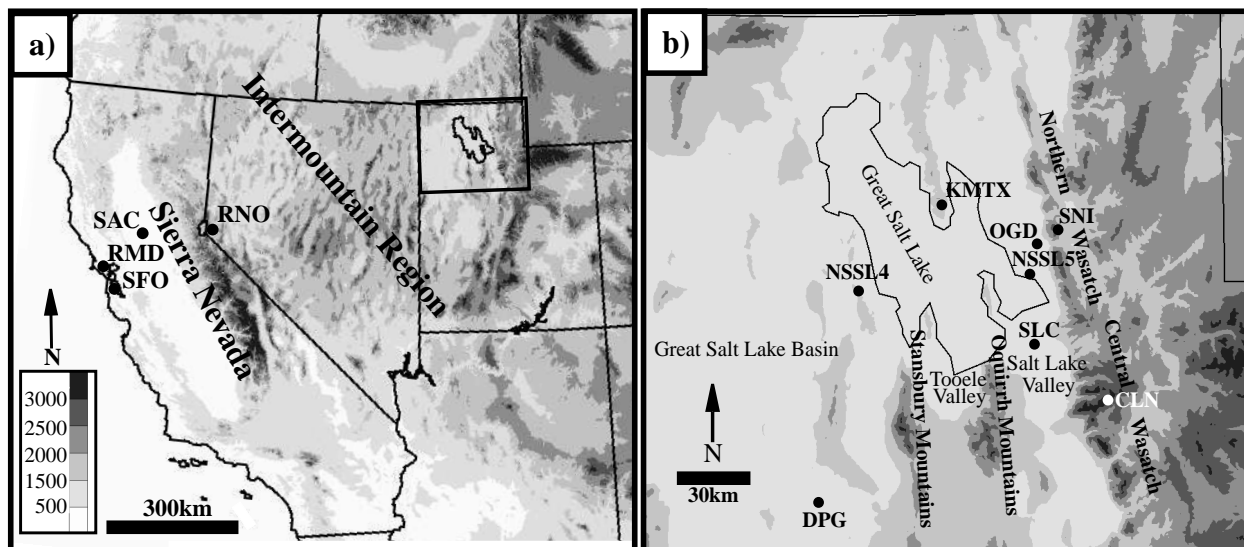


Figure 1. Topography and major geographic features of (a) the western United States and (b) northern Utah. Elevation (m) based on scale at lower left in (a). Boxed area in (a) identifies location of IPEX target area in (b).



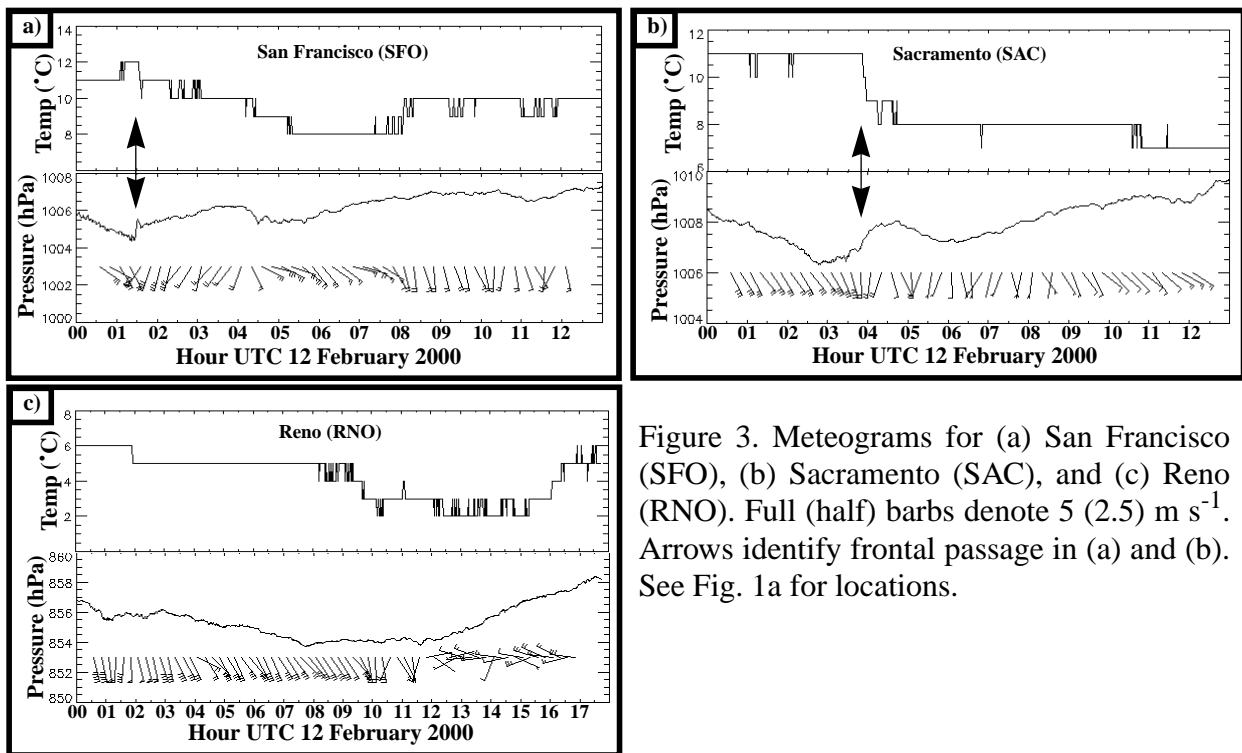


Figure 3. Meteorgrams for (a) San Francisco (SFO), (b) Sacramento (SAC), and (c) Reno (RNO). Full (half) barbs denote 5 (2.5)  $\text{m s}^{-1}$ . Arrows identify frontal passage in (a) and (b). See Fig. 1a for locations.

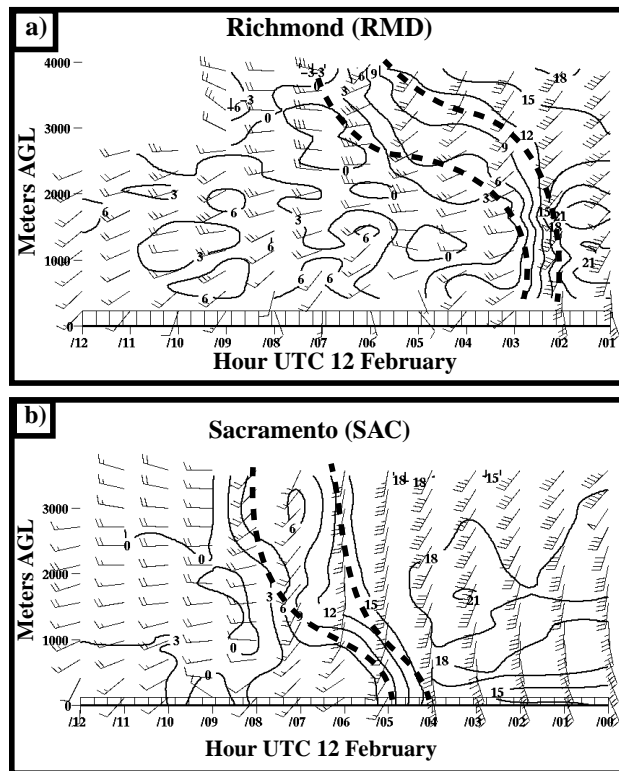


Figure 4. Wind profiler data for 12 February 2000 from (a) Richmond (RMD) and (b) Sacramento (SAC). Full (half) barb denote 5 (2.5)  $\text{m s}^{-1}$ . Meridional wind component plotted every 3  $\text{m s}^{-1}$  as solid lines. Dashed lines denote wind shear accompanying frontal zone. See Fig. 1a for locations.

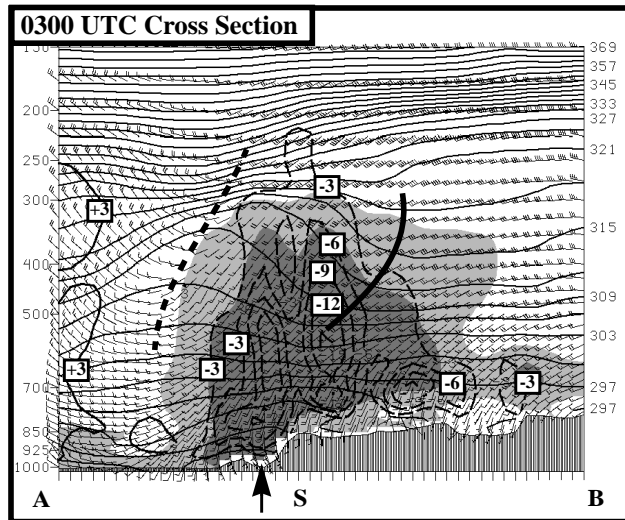


Figure 5. RUC2 cross section along line AB of Fig. 2b at 0300 UTC 12 Feb. Potential temperature (thin lines every 3K), vertical velocity ( $\omega$ , thick lines every  $3 \times 10^{-1} \text{ Pa s}^{-1}$  with negative contours dashed), wind [full (half) barbs denote 5 (2.5)  $\text{m s}^{-1}$ ], and relative humidity (light, dark shading denote >70 and 90%, respectively). Upper-level trough axis denoted by heavy dashed line, leading edge of upper-level baroclinic zone denoted by heavy solid line, and surface front position denoted by arrow. Sierra Nevada indicated by S.

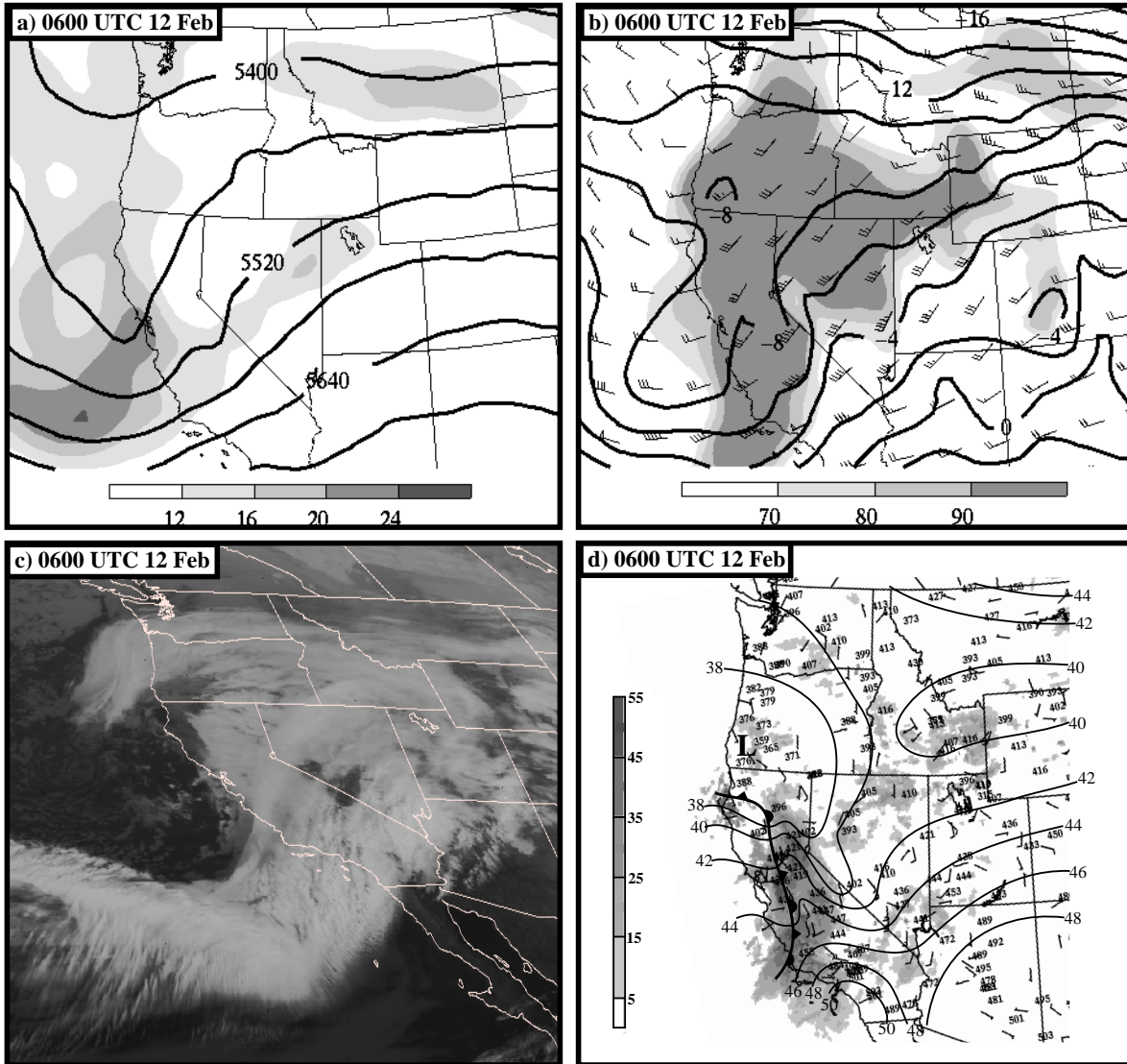


Figure 6. Same as Fig. 2 except for 0600 UTC 12 Feb 2000.

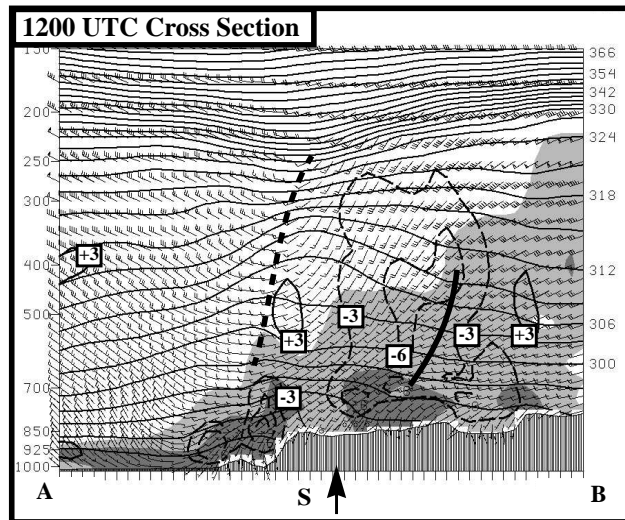


Figure 7. Same as Fig. 5 except for 1200 UTC 12 Feb 2000 and arrow denotes surface pressure trough position.

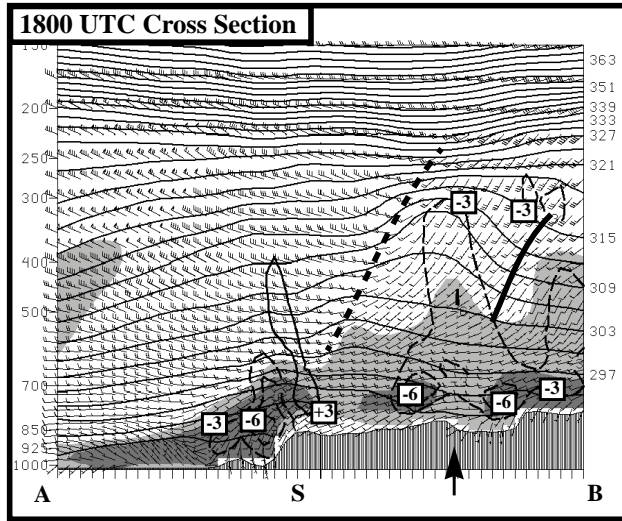


Figure 8. Same as Fig. 5 except for 1800 UTC 12 Feb 2000 and arrow denotes position of surface pressure trough.

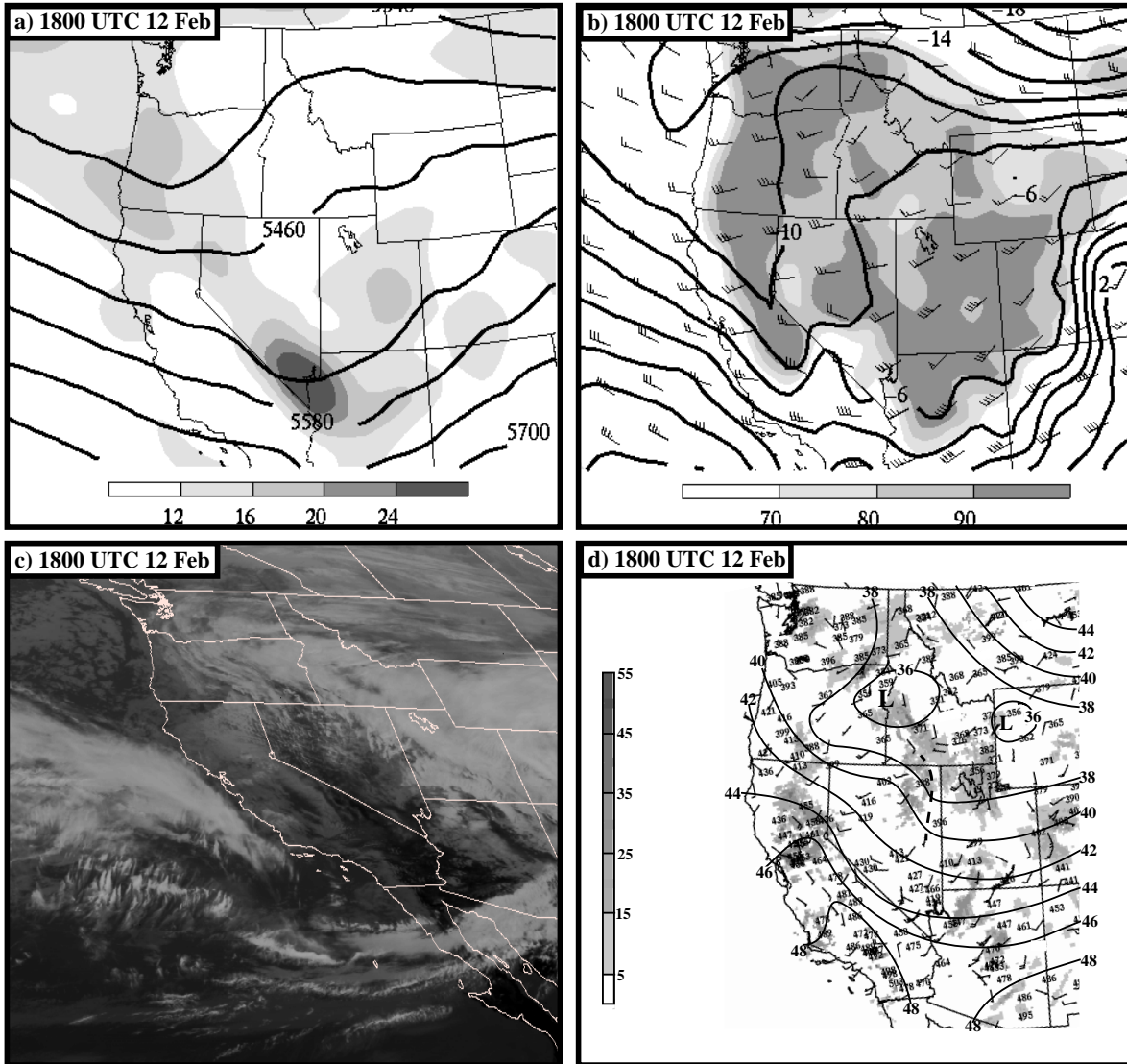


Figure 9. Same as Fig. 2 except for 1800 UTC 12 February 2000.

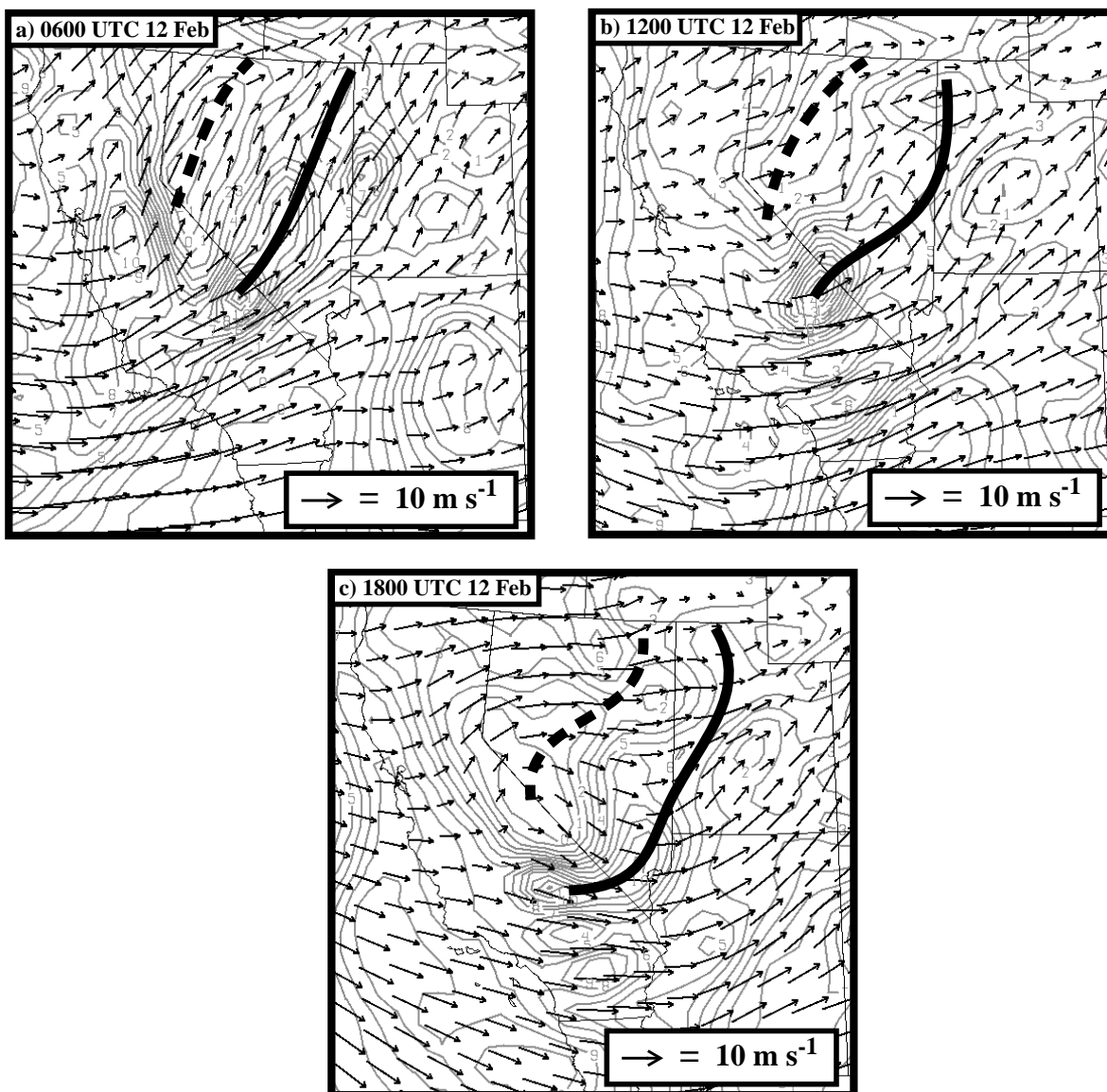


Figure 10. EDAS 700-hPa potential vorticity (every  $1 \times 10^{-7} \text{ m}^2 \text{ s}^{-1} \text{ K kg}^{-1}$ ) and wind (vector scale at lower right). High (low) potential vorticity banners denoted by thick solid (dashed) line. (a) 0600 UTC 12 Feb 2000. (b) 1200 UTC. (c) 1800 UTC.

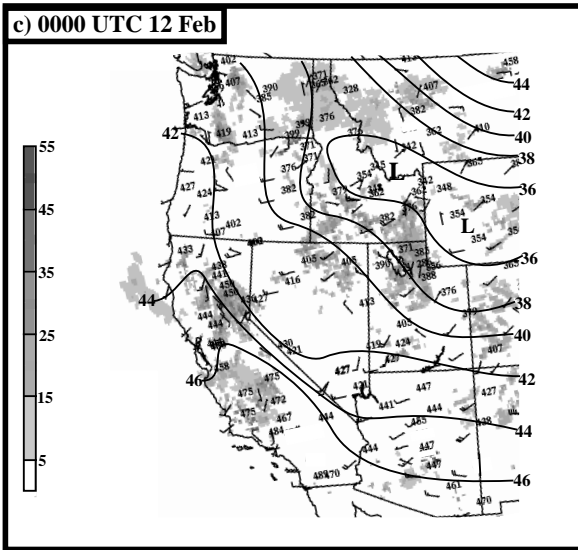
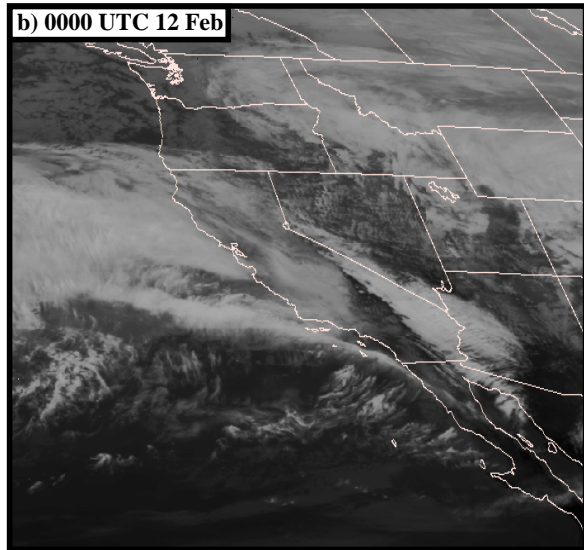
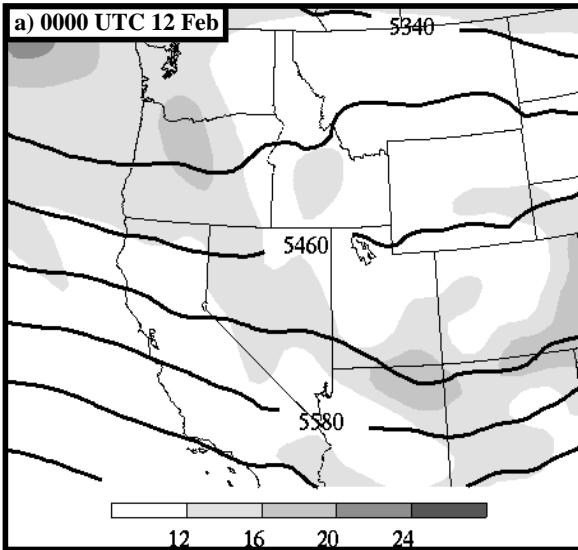


Figure 11. Same as (a) Fig. 2a, (b) Fig. 2c, and (c) Fig. 2d, except for 0000 UTC 13 Feb 2000.

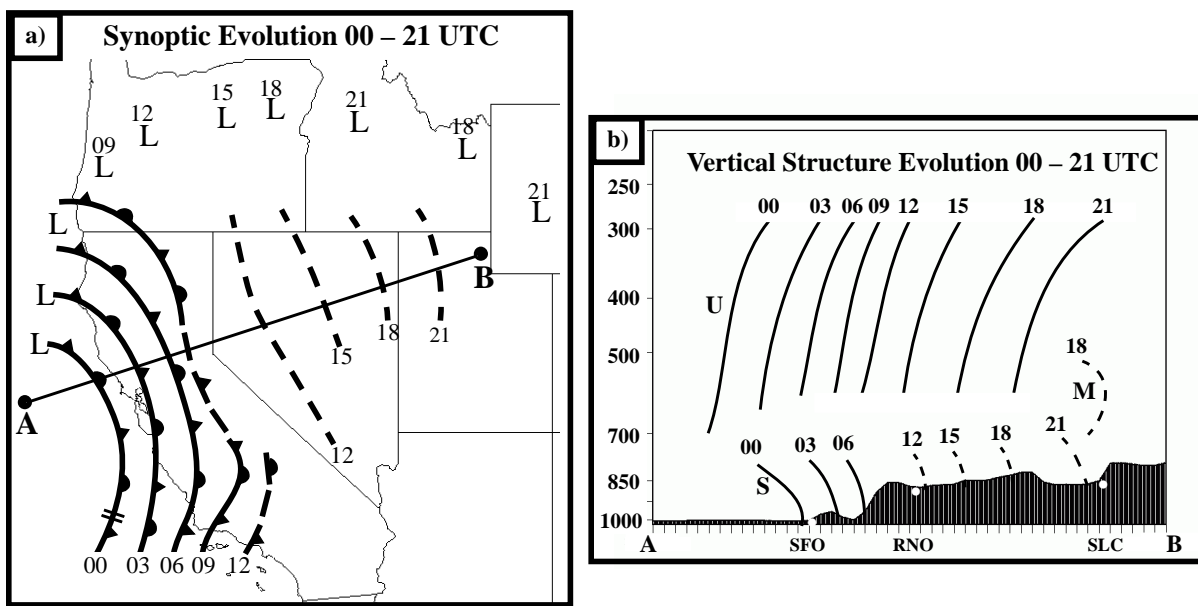


Figure 12. Summary of surface and vertical structure evolution of IOP3. (a) Surface features every 3 h (conventional symbols) from 0000–2100 UTC 12 Feb 2000. Labels represent hour UTC. (b) Vertical trough structure (roughly along line AB of Fig. 2b) every 3 h. U denotes upper level trough, S surface trough, and M midlevel trough.

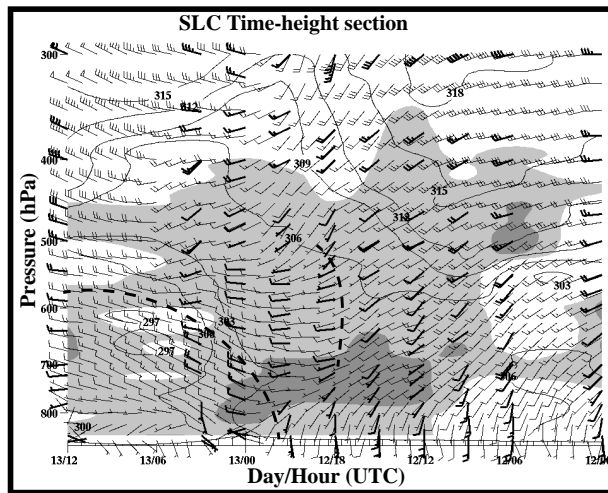


Figure 13. Salt Lake City (SLC) time-height section based on 3-h soundings (thick barbs) with RUC2 winds (thin barbs) overlaid.  $\theta_e$  (solid lines, every 3 K), relative humidity (light and dark shading denote >70 and 90%, respectively), and wind [full (half) barbs denote 5 and (2.5)  $\text{m s}^{-1}$ ]. Dashed lines denote mid-level and surface-based troughs.

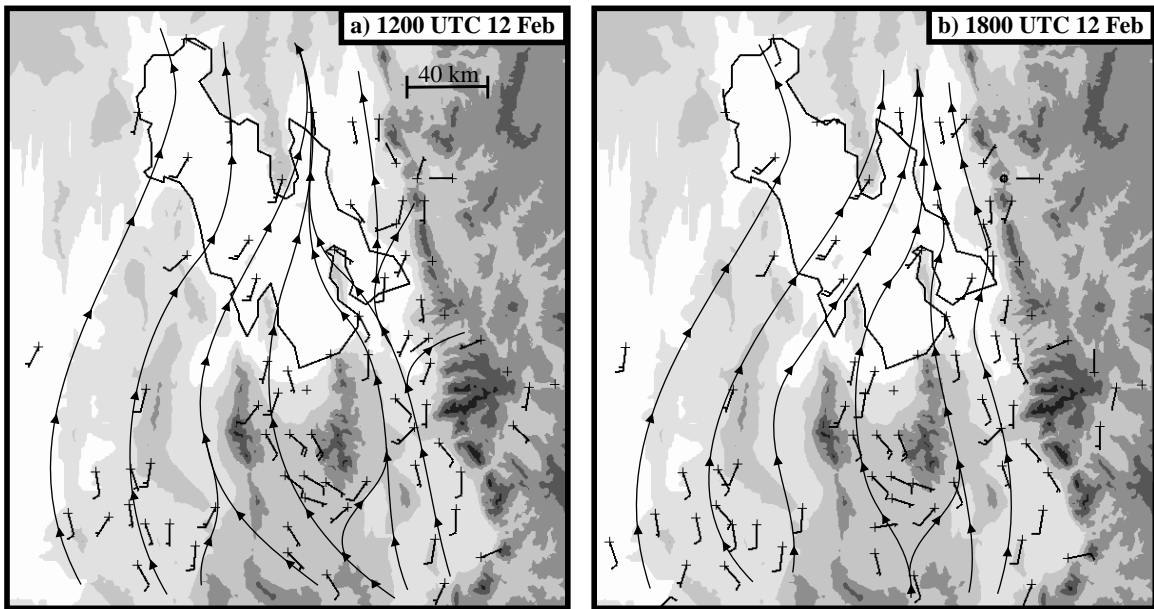


Figure 14. Northern Utah manual streamline analysis at (a) 1200 and (b) 1800 UTC 12 Feb 2000. Station data and streamlines for elevations between 1280–2200m AMSL (roughly at and below mid mountain). Full (half) barbs denote 5 (2.5)  $\text{m s}^{-1}$ .

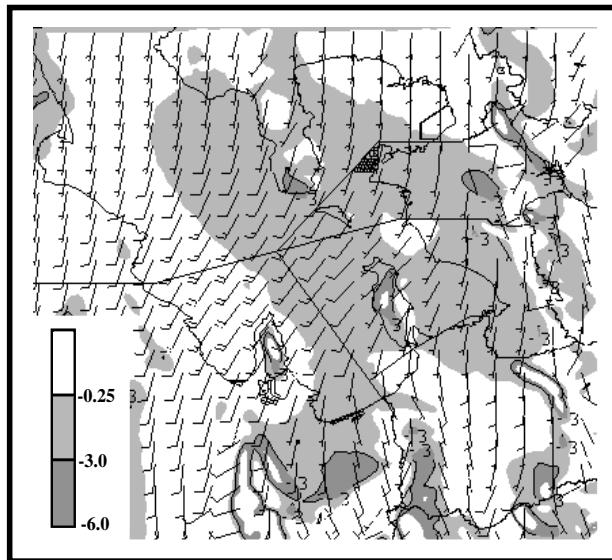


Figure 15. ARPS Data Assimilation System (ADAS) surface analysis at 1800 UTC 12 Feb 2000, surface divergence (light and dark shading denote less than  $-0.25 \times 10^{-4} \text{ s}^{-1}$  and  $-3.0 \times 10^{-4} \text{ s}^{-1}$ , respectively) and wind [full (half) barbs denote 5 (2.5)  $\text{m s}^{-1}$ ].

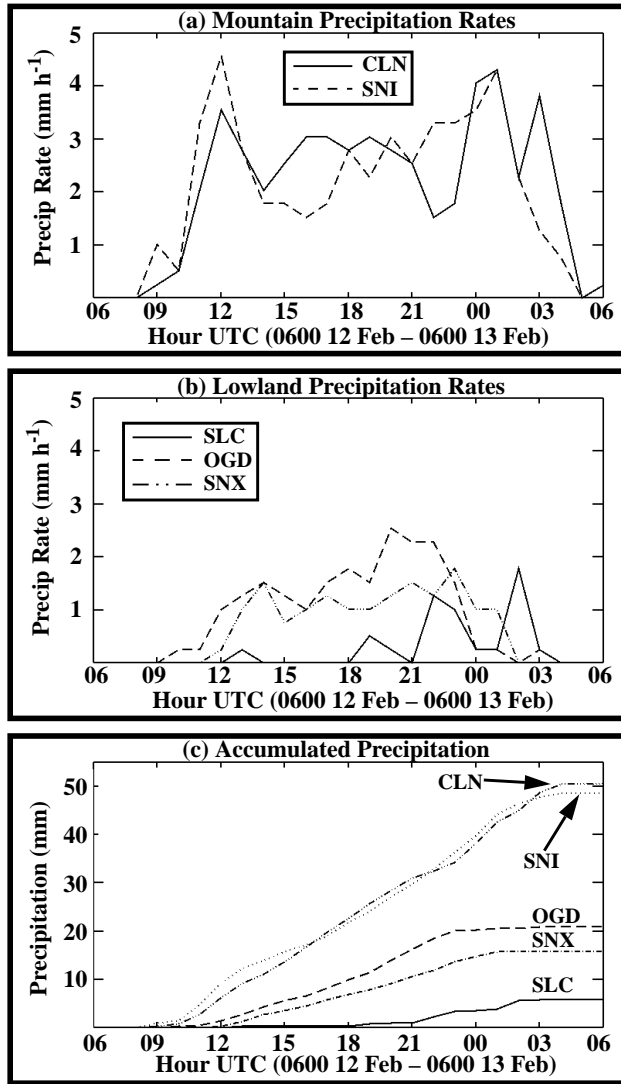


Figure 16. Precipitation rates and accumulated precipitation at selected locations. (a) Mountain precipitation rates ( $\text{mm h}^{-1}$ ). (b) Lowland precipitation rates ( $\text{mm h}^{-1}$ ). (c) Accumulated precipitation (mm). See Fig. 1b for locations.

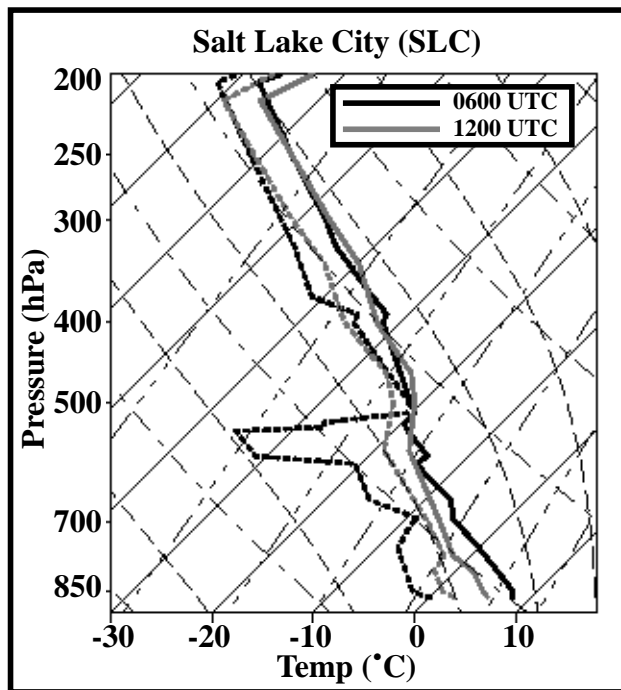


Figure 17. Skew T–logp diagram [temperature (solid) and dewpoint (dashed)] at SLC for 0600 UTC (black) and 1200 UTC (gray) 12 Feb 2000.

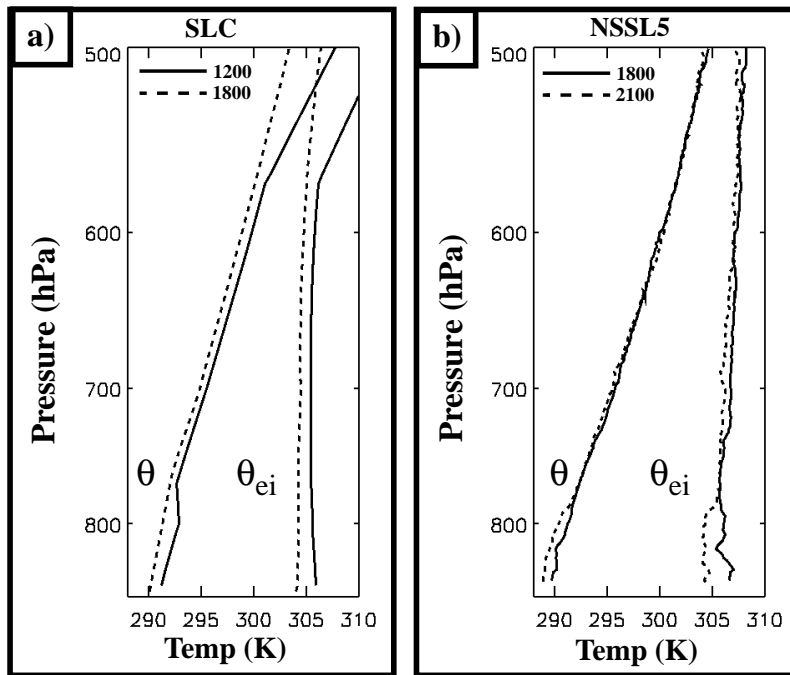


Figure 18. Vertical profiles of potential (left) and equivalent potential temperature with respect to ice (right) at (a) SLC and (b) NSSL5. See Fig. 1b for locations.

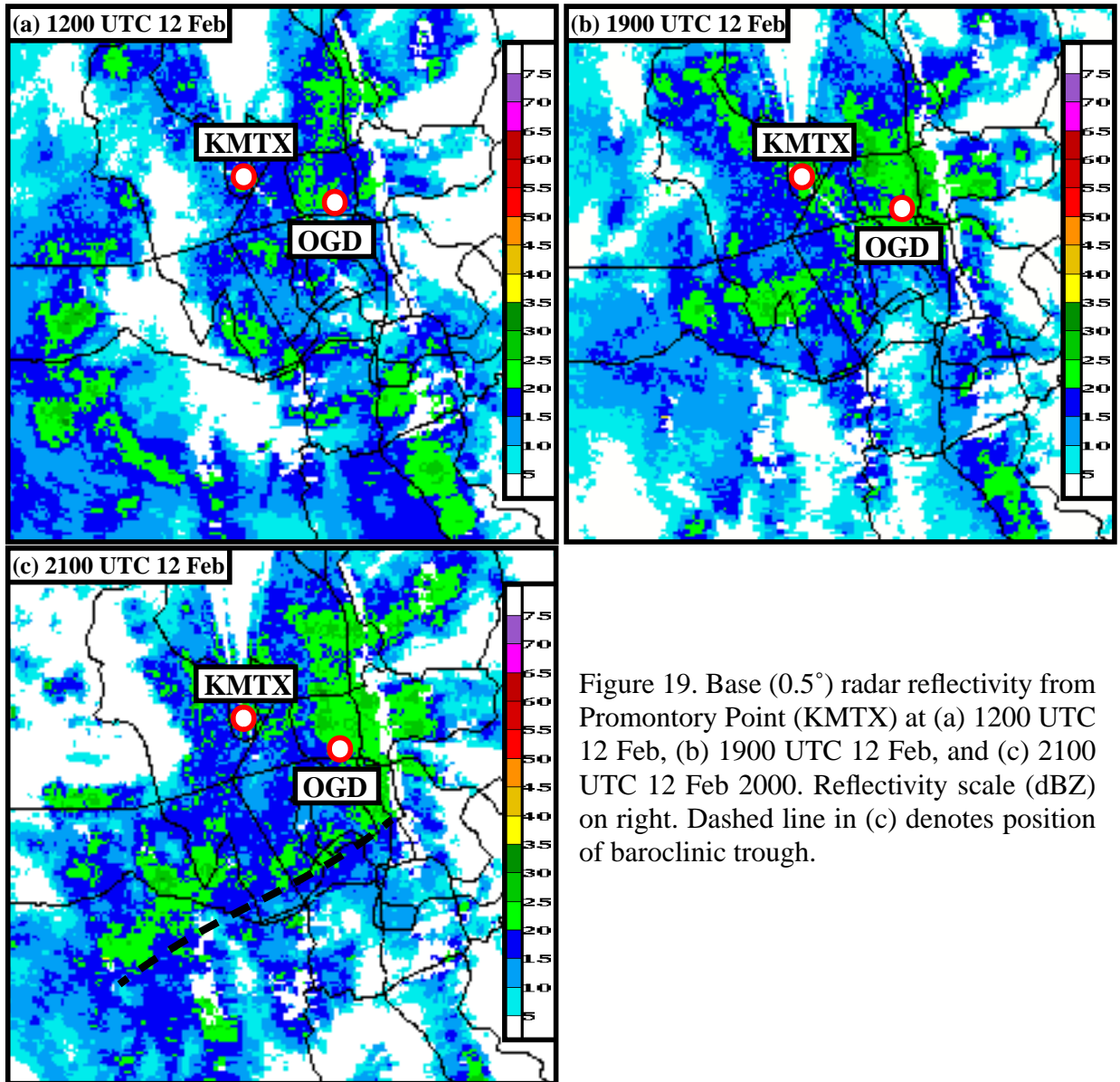


Figure 19. Base ( $0.5^\circ$ ) radar reflectivity from Promontory Point (KMTX) at (a) 1200 UTC 12 Feb, (b) 1900 UTC 12 Feb, and (c) 2100 UTC 12 Feb 2000. Reflectivity scale (dBZ) on right. Dashed line in (c) denotes position of baroclinic trough.

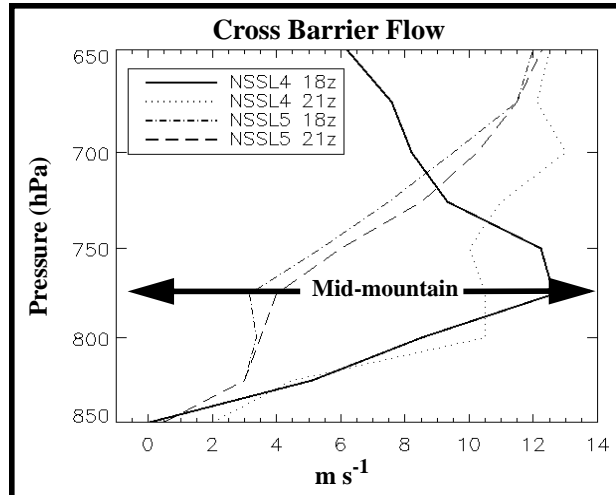


Figure 20. Cross-barrier flow magnitude ( $\text{m s}^{-1}$ ) at NSSL4 and NSSL5 for 1800 and 2100 UTC 12 Feb 2000. See Fig. 1b for locations.

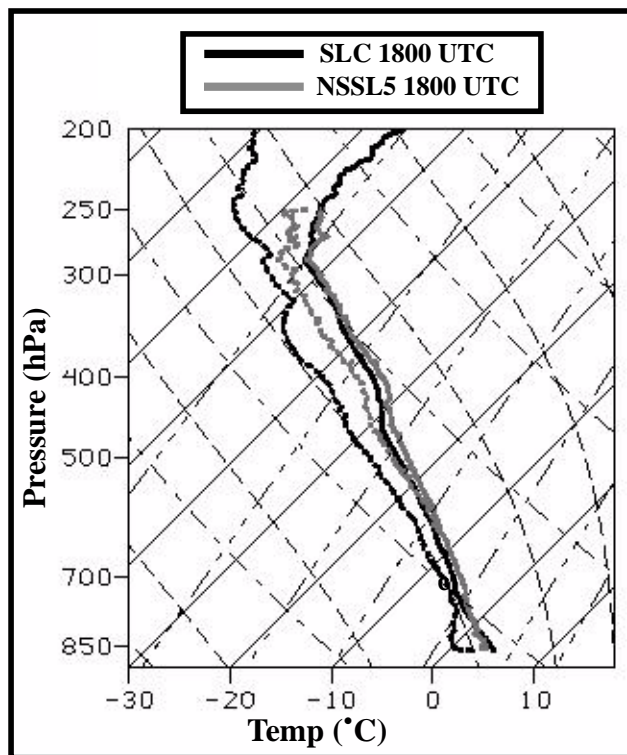


Figure 21. Skew T–log p diagram [temperature (solid) and dewpoint (dashed)] at SLC and NSSL5 for 1800 UTC 12 Feb 2000.

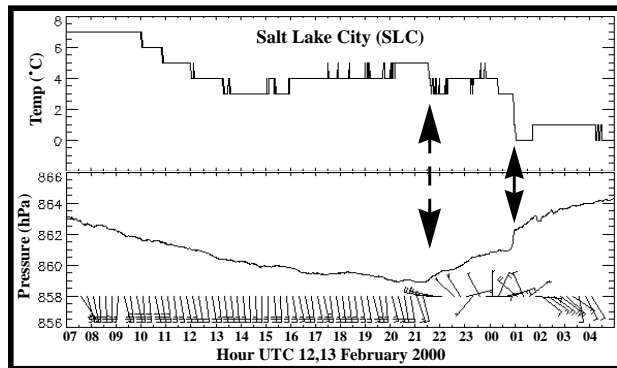


Figure 22. Same as in Fig. 3 except for SLC. Arrows denote the passage of the baroclinic trough (dashed) and convective line (solid). See Fig. 1b for location.

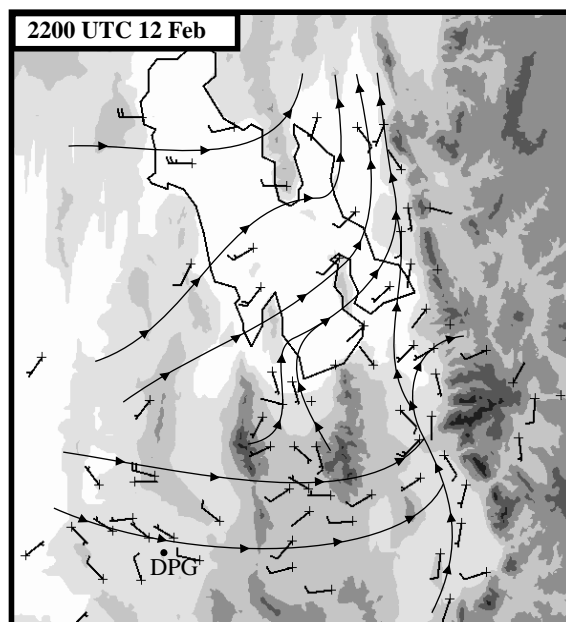


Figure 23. Same as Fig. 14 except for 2200 UTC 12 Feb 2000.

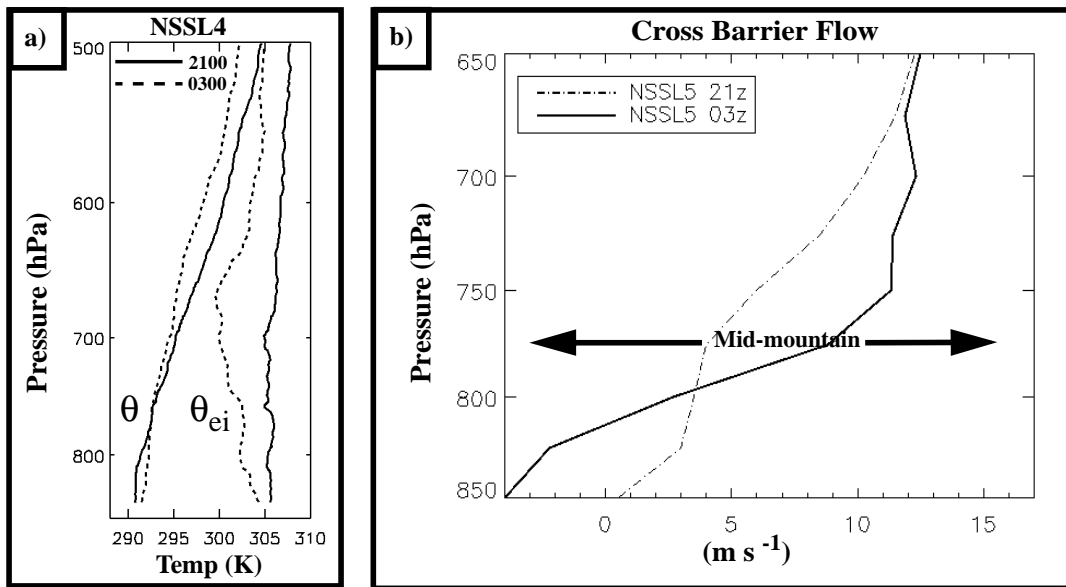


Figure 24. (a) Vertical profiles of potential and equivalent potential temperature with respect to ice at NSSL4 at 2100 and 0300 UTC 13 Feb. (b) NSSL5 cross barrier flow at 2100 and 0300 UTC 13 Feb.



